Variations of Joint Integrated Data Association With Radar and Target-Provided Measurements

AUDUN G. HEM
EDMUND F. BREKKE

Target tracking algorithms are usually based on exteroceptive measurements obtained from sensors placed in the center of some surveillance area. However, information transmitted from surrounding targets will often also be available. This information, here dubbed target-provided measurements, will often include valuable information for a tracking system. We present a multitarget tracking algorithm utilizing such measurements using a framework of joint integrated data association. The use case we consider is maritime target tracking using radar measurements combined with messages from the automatic identification system. The full details of the tracking algorithm are presented, including implementation-specific considerations to account for the different natures of the incoming measurements. We detail three different methods of handling the target-provided measurements: one processing them as they arrive, i.e., sequentially, and the others collecting and processing them at fixed intervals. The results show that all three improve over the pure radar tracking algorithm and similar state-of-the-art methods.

Manuscript received January 19, 2022; revised January 26, 2023; released for publication March 20, 2023.

Audun G. Hem and Edmund F. Brekke are with the Department of Technical Cybernetics, Norwegian University of Science and Technology, 7034 Trondheim, Norway (e-mail: audun.g.hem@ntnu.no; edmund.brekke@ntnu.no).

Refereeing of this contribution was handled by Ting Yuan.

This work was supported in part by the Research Council of Norway through Projects 223254 AMOS, 309230 SFI Autoship and 295033 Autosit, in part by DNV, in part by Kongsberg, and in part by Maritime Robotics.

I. INTRODUCTION

One of the many important puzzle pieces for increased degrees of autonomy in the maritime sector is the ability of a ship to observe its surroundings. To avoid collisions and safely navigate the waters, it is necessary to know where the surrounding ships are situated. For this to work safely and robustly, target tracking algorithms have to provide precise estimates of the position and direction of surrounding vessels, also known as targets. Radar-based target tracking algorithms have largely been the norm when navigating outside of close encounter harbor areas. There is, however, also a standardized system to help with collision avoidance at sea: the automatic identification system (AIS). This system provides target-provided measurements with valuable information that could help give better estimates than what only radar measurement can provide. However, this valuable source of information often remains unused in modern target tracking algorithms.

When monitoring aircraft, target-provided measurements are also used, with measurements based on the automatic dependent surveillance–broadcast (ADS-B) protocol. The latter protocol can, together with radar, be used in air traffic control to provide a better picture of the airspace [4]. The availability of target-provided measurements makes it possible to identify targets and utilize information that is impossible to get from radar measurements alone, such as the ship destination. For, e.g., long-time vessel prediction, the additional information provided by target-provided measurements can be very valuable [31].

The two measurement types are inherently different. The radar is attached to the ship, scanning the surrounding area. The measurements are unlabeled, can be false alarms, and can provide several detections for each target. The last issue is often solved using a clustering algorithm, while the problem of false alarms has no single simple solution. The radar measurements are also often noisier than the target-provided measurements, with the noise becoming more prominent when the target is far away. Target-provided measurements, on the other hand, are sent out from the surrounding ships as data packages containing not only the position of the target but additional information as well, such as the ID number of the transmitting ship. Because a target needs to send a target-provided measurement for it to be received, there are no false alarms, and the precision of the transmitted kinematic information is independent of the distance to the target because the positional data comes from GPS measurements. However, not all targets have a transmitter, and the messages will often be received somewhat infrequently, as high-frequency transmitting is not always required, see, e.g., [19]. Thus, a robust target tracking system based only on target-provided measurements will not be feasible.

There are two established approaches to the fusion of sensor signals: track-to-track fusion and track-to-measurement fusion [1]. Here track-to-measurement fusion is examined, and a model suitable for incorporating target-provided measurements, and a tracking algorithm utilizing this model, is presented. For example, Gaglione *et al.* [13] have previously investigated track-to-measurement fusion for radar and target-provided information. The tracking algorithm presented here differs from previous work in some significant ways. We use a hybrid state framework based on [7], which can include motion and visibility models in addition to target IDs. Furthermore, building upon [7], we derive the tracking algorithm as a special case of the Poisson multi-Bernoulli mixture (PMBM) filter originally proposed in [34]. An important technical detail to enable this is to model the birth model as a marked Poisson point process (PPP), where the target IDs take the role of the marks. The resulting algorithm can be seen as a generalized version of joint integrated probabilistic data association (JIPDA) [24].

The contributions of this paper are as follows. It derives a framework that includes target-provided measurements based on a PMBM formulation of the JIPDA. The resulting target tracker includes both a visibility state and multiple kinematic models. Furthermore, the paper details a sequential way of handling the incoming target-provided measurements, a method more similar to the one described in [13], and a method similar to how radar measurements are processed. Lastly, we present some implementation-specific considerations to make when handling target-provided measurements in a tracker.

The paper is organized as follows: We detail the problem formulation in Section III. In Section IV, we explain the structure of the hybrid state that facilitates the inclusion of target-provided information. We present the mathematical expressions needed for calculations in Section V. In Section VI, three different methods for handling the incoming measurements are detailed. Section VII presents the implementation choices, together with considerations to make to accommodate the target-provided measurements. Lastly, Section VIII presents the results. We compare the performance of the different measurement handling methods and how they compare to using only radar and the method from [13].

II. BACKGROUND

This work builds upon the multitarget tracking method presented in [7] and can be considered an extension of the framework described there. The tracking algorithm, denoted as visibility interacting multiple models joint integrated probabilistic data association (VIMMJIPDA), combines interacting multiple models (IMM) and a visibility state with the well-established JIPDA framework. The tracking method was derived with a basis in the PMBM filter [34].

Darko Musicki and Rob Evans introduced the JIPDA in [24], where the concept of visibility is mentioned and indicates whether the tracked target is visible to the sensor or not. Later, e.g., [35] has explored visibility in connection with the problem of estimating target detectability. The JIPDA is an extension of the joint probabilistic data association (JPDA) method developed by Yaakov Bar-Shalom [12], which again is an extension of Bar-Shalom's probabilistic data association (PDA) method [3]. These methods are well established in the target tracking community and have been used for a range of different purposes, such as collision avoidance for marine vessels [29], autonomous navigation [11], and air traffic control [20]. Henk A. P. Blom and Yaakov Bar-Shalom introduced the IMM method [5], and it has been used for several decades in, e.g., air traffic control. Furthermore, Musicki and Suvorova presented an IMM-JIPDA algorithm in [25].

The PMBM filter and subsequent tracking algorithms [15] utilize the PMBM density, which is the union between a PPP and a multi-Bernoulli mixture (MBM). The PPP represents unknown targets, i.e., undetected targets hypothesized to exist, and the MBM represents already detected targets. Links between PMBM and JIPDA have been established in [34] (single kinematic model, loopy belief propagation as an alternative to hypothesis enumeration) and in [7] (multiple kinematic models, standard hypothesis enumeration, and mixture reduction).

Some work on the track-to-measurement fusion of radar and target-provided measurements has been done previously, both by Habtemariam *et al.* [17] and Gaglione *et al.* [13]. The first approach includes target-provided measurements in a JPDA-like tracking algorithm, while the second uses a framework that also includes track existence. The second approach utilizes probabilistic graphical models and loopy belief propagation for the calculations. Furthermore, Gaglione *et al.* use particle filtering for performing the calculations. Both works perform data association on batches of target-provided measurements simultaneously as on the radar measurements. Gaglione *et al.* nevertheless consider that target-provided measurements can arrive at any time. They also share similar modeling of the target-provided measurement IDs, from which the model presented here deviates. However, neither method directly addresses the initialization of tracks using target-provided measurements. In [21], a multiple hypothesis tracking (MHT) approach is presented, which also showed promising results but relied on preprocessing of the AIS measurements. Track-to-track fusion using radar and AIS measurements has also been done previously, e.g., in [9]. Here, a multisensor network for maritime surveillance is described, utilizing several sensors, including radar and AIS. More recently, research has been conducted into the track-to-track association of radar- and AIS-tracks [27].

III. PROBLEM FORMULATION

The unknown target intensity $u(\mathbf{y})$ describes the not yet discovered targets present in the surveillance area. We model the unknown targets as a marked PPP, which is equivalent to a PPP on the Cartesian product of the space $\mathbf{R}^{n_x}$ and the discrete spaces the discrete hybrid states can take values from [30, p. 205]. In its general form, this process is

$$b(\mathbf{y}) = p(v)p(\tau|v)p(s|v,\tau)p_\gamma(\mathbf{x}|s,v,\tau), \tag{1}$$

where $p_\gamma(\mathbf{x}|s,v,\tau)$ is an intensity function on the the space $\mathbf{R}^{n_x}$, and $p(\cdot)$ are distributions over the discrete states. Rather than using the birth intensity directly, we use Proposition 1 from [7] to get the converged unknown target intensity

$$u(\mathbf{y}) = U o_u^v \xi_u^\tau \mu_u^\tau f_u(\mathbf{x}). \tag{2}$$

Here, U is the overall birth rate of new targets, o_u^v is the probability of visibility state v, ξ_u^τ is the probability of ID τ, μ_u^τ is the probability of the kinematic mode s, and $f_u(\mathbf{x})$ is the distribution of the kinematic state. The subscript u indicates that the individual expressions are part of the unknown target intensity. Equation (2) does not contain the initial values of new targets, as it is a function of the birth intensity and the transition probability matrices. However, for simplicity, the unknown target values are tuned directly and can be viewed as initial values.

Remark 1. This method of modeling the target IDs through a marked PPP implies that two targets can have the same ID. The probability of two targets having the same ID in a surveillance area with relatively few targets is minuscule, but it is nevertheless a possibility [10]. We also note how the modeling of actual, observable IDs here deviates from theoretically assigned IDs. The labels in labeled random finite sets (RFSs), introduced in [32], are unobservable and analogous to the identifying tags in [14], which ensure the uniqueness of the elements of a RFS. The IDs described here, however, serve no such purpose and can be assumed nonunique without breaking the underlying mathematical assumptions of RFSs.

M2: We model the survival probability as a function of time since the last update. A constant parameter P_{S_c} denotes the probability of survival after one second. Thus, the survival probability of an interval between times t_{k-1} and t_k, denoted as Δt, becomes

$$P_S(\Delta t) = P_{S_c}^{\Delta t}. \tag{3}$$

M3: The ID numbers τ are assumed to be static, in line with the physical reality of the AIS protocol. The IDs are manually set at the installation of the AIS system. We assume that the ID numbers of the unknown targets are distributed according to

$$\xi_u^\tau = \begin{cases} \xi_u^0 & \text{if } \tau = 0 \\ \dfrac{1-\xi_u^0}{|\mathcal{V}|-1} & \text{if } \tau > 0 \end{cases}, \tag{4}$$

where ξ_u^0 is some parameter denoting the belief that the target has no ID and $|\mathcal{V}|$ is the number of all possible ID numbers in addition to 0. Not all targets have an ID, and we represent this non-ID by the value $\tau = 0$. If $\tau = 0$, the target does not transmit measurements.

M4: From time step $k-1$ to k, the evolution of a target is given by

$$f_{\mathbf{y}}(\mathbf{y}_k|\mathbf{y}_{k-1}) = f_{\mathbf{x}}^{s\tau}(\mathbf{x}_k|\mathbf{x}_{k-1})\pi^{s_{k-1}s_k} w^{v_{k-1}v_k}. \tag{5}$$

The π-matrix contains the Markov chain probabilities of changing between different kinematic models. The matrix w contains the Markov chain probabilities of the target switching between the visible state $v = 1$ and invisible state $v = 0$. The ID numbers are assumed static and therefore do not change during a prediction.

M5: For radar measurements, the detection probability $P_D(\mathbf{y}_k)$ varies based on the visibility state v, and we define it as

$$P_D(\mathbf{y}_k) = \begin{cases} P_D & \text{if } v = 1 \\ 0 & \text{if } v = 0 \end{cases}, \tag{6}$$

where P_D is a constant describing the probability of a target being detected by the radar at a given time step.

For target-provided measurements, which are assumed to give no missed detections, we have that

$$P_D(\mathbf{y}_k) = \begin{cases} 1 & \text{if a target-provided measurement} \\ & \quad \text{is received} \\ 0 & \text{otherwise} \end{cases} \tag{7}$$

independent of the visibility state. Thus, no conclusions about a target are made from the absence of target-provided measurements. Trying to keep track of when a vessel should transmit measurements is a difficult problem that, e.g., would be subject to intentional randomness from the protocol [6].

M6: Radar clutter measurements are assumed to follow a Poisson process with intensity λ. The target-provided measurements do not contain clutter, the same as if they are following a Poisson process with intensity 0.

M7: The radar measurements are assumed to be synchronized and to arrive simultaneously at a fixed frequency. The synchronicity means that when radar measurements arrive at time step k, the set of radar measurements contains measurements from all detected targets at time step k, in addition to clutter measurements. The radar measurement likelihood is denoted as $f_{\mathbf{z}}^R(\mathbf{z}_k|\mathbf{y}_k)$.

M8: The target-provided measurements can arrive whenever and are not synchronized. Thus, a transmitted measurement can be received at any time from any target. We do not assume that targets transmit measurements simultaneously, contrary to what we do for radar measurements. Whenever a target-provided measurement arrives, however, the time of arrival is assumed to be known. The measurement likelihood for the target-

provided measurements is

$$f_{\mathbf{z}}^{A}(\mathbf{z}_k|\mathbf{y}_k) = f_{\mathbf{p}}(\mathbf{p}_k|\mathbf{y}_k) f_{\tau}(\tau^{\mathbf{z}_k}|\tau), \tag{8}$$

where $\mathbf{z}_k$ is the whole measurement and $\mathbf{p}_k$ only contains the kinematic data of the measurement. Furthermore,

$$f_{\tau}(\tau^{\mathbf{z}_k}|\tau) = \begin{cases} P_C & \text{if } \tau_k = \tau_k^{\mathbf{z}_k} \\ \dfrac{1-P_C}{|\mathcal{V}|-1} & \text{if } \tau_k \neq \tau_k^{\mathbf{z}_k} \text{ and } \tau > 0, \\ 0 & \text{if } \tau = 0 \end{cases} \tag{9}$$

where P_C is a fixed parameter describing the confidence in the ID number not being corrupted, denoted as the confidence probability. The reasoning behind the above equation comes from the observation that the likelihood of a transmitted measurement coming from a target without an ID is zero. Furthermore, the chance of a transmitted ID being erroneous makes it a possibility, albeit small, that any ID can be the correct one.

IV. HYBRID STATES AND THE PMBM

As formulated in [2, p. 441], a hybrid state is a state where the state space contains both discrete and continuous states or uncertainties. This structure is useful as the kinematic state will be continuous, while, e.g., the choice of kinematic model for the target will be discrete.

A PMBM filter represents the posterior multitarget density for discovered targets as a weighted sum of multi-Bernoulli densities. These involve weights for each of the multi-Bernoullis, and kinematic densities and existence probabilities for each of the Bernoullis. The PMB filter, which is essentially the same as a JIPDA, approximates the sum of multi-Bernoullis by a single multi-Bernoulli at the end of each estimation cycle.

Using the equations from [34], one can get general expressions for the weight, existence, and states irrespective of the sensor type, assuming the sensors generate measurements adhering to the assumptions made in Assumption 2 in [34]. The assumptions hold for both target-provided and radar measurements. The inclusion of IDs in the target-provided measurements is contained in the measurement likelihood function, and they do not breach any independence assumptions. The goal of this section is to extract expressions for the probabilistic properties of the individual hybrid state elements.

From [34], we have that the weight w, existence probability r, and distribution $f(\mathbf{y})$ of a single Bernoulli in general can be written as

$$w = g(\mathbf{y}) + h[1], \tag{10}$$

$$r = \frac{h[1]}{g(\mathbf{y}) + h[1]}, \tag{11}$$

$$f(\mathbf{y}) = \frac{h(\mathbf{y})}{h[1]} \tag{12}$$

for some functions g and h of the state $\mathbf{y}$. The notation $[\cdot]$ indicates a linear functional, defined as

$$g[h] = \int g(\mathbf{x}) h(\mathbf{x}) d\mathbf{x}. \tag{13}$$

These are useful tools for compactly writing normalization constants and likelihoods. For later use, it is convenient to find general expressions for the individual states in the hybrid state $\mathbf{y}$. Using the approximation from [7, Remark 6] that the visibility is independent on the other states, we can write $h(\mathbf{y}) = h(v)h(\tau)h(s|\tau)h(\mathbf{x}|\tau, s)$. We get the individual states by using the rule of conditional probability. Starting with the kinematic state $\mathbf{x}$, it can be acquired by

$$\begin{aligned} f^t(\mathbf{x}|s, \tau, v) &= \frac{f(\mathbf{x}, s, \tau, v)}{\int f(\tilde{\mathbf{x}}, s, \tau, v) \mathrm{d}\tilde{\mathbf{x}}} \\ &= \frac{\dfrac{h(\mathbf{x}, s, \tau, v)}{h[1]}}{\dfrac{\int h(\tilde{\mathbf{x}}, s, \tau, v) \mathrm{d}\tilde{\mathbf{x}}}{h[1]}} \\ &= \frac{h(\mathbf{x}, s, \tau, v)}{\int h(\mathbf{x}, s, \tau, v) \mathrm{d}\mathbf{x}} \\ &= \frac{h(v)h(\mathbf{x}, s, \tau)}{h(v) \int h(\tilde{\mathbf{x}}, s, \tau, v) \mathrm{d}\tilde{\mathbf{x}}} \\ &= \frac{h(\mathbf{x}, s, \tau)}{h(s, \tau)}, \end{aligned} \tag{14}$$

where we have omitted the time indices for brevity. The $\tilde{(\cdot)}$ notation is used for latent variables, which disappear by marginalization. Furthermore, the absence of the visibility state v in the final expression means that $f^t(\mathbf{x}|s, \tau, v) = f^t(\mathbf{x}|s, \tau)$. Similarly, the mode probabilities are

$$f^t(s|\tau) = \mu^{t\tau s} = \frac{h(s, \tau)}{h(\tau)}, \tag{15}$$

the ID probabilities are

$$f^t(\tau) = \xi^{t\tau} = \frac{h(\tau)}{h[1]}, \tag{16}$$

and the visibility probabilities are

$$f^t(v) = o^{tv} = \frac{h(v)}{h[1]}. \tag{17}$$

Note that $\sum_{\tilde{\tau}} \sum_{\tilde{s}} \int h(\tilde{\mathbf{x}}, \tilde{s}, \tilde{\tau}) \mathrm{d}\tilde{\mathbf{x}} = h[1]$, which essentially acts as a normalization constant. Independencies between the states will make it possible to reduce the needed amount of marginalization, as they will appear both in the numerator and the denominator. The independencies will depend on the model choices and are written here according to the assumptions in Section III.

V. INCLUDING TARGET-PROVIDED MEASUREMENTS IN THE VIMMJIPDA

In the VIMMJIPDA, the unknown target intensity $u(\mathbf{y})$ is assumed stationary and is left unchanged during the prediction and updating of the estimates. We make the same assumption here. This assumption means that only the Bernoulli components have to be considered, and is further simplified by following the JIPDA method of performing mixture reduction. That is, we merge all Bernoullis originating in the same measurement into a single Bernoulli after each update. Thus, we can omit the weights of the association hypotheses of previous time steps can due to marginalization. Table II shows the expressions for updating and predicting the Bernoulli components from [34]. These are adapted to simplify insertion in (10)–(12) and (14)–(17). Furthermore, they are simplified to reflect the stationary unknown target intensity and the marginalization over the weights during mixture reduction. As the measurement model assumptions made in [34] hold with regards to both radar and target-provided measurements, both $f_{\mathbf{z}}^{R}(\mathbf{z}|\mathbf{y})$ and $f_{\mathbf{z}}^{A}(\mathbf{z}|\mathbf{y})$ can be considered special cases of the more general $f_{\mathbf{z}}(\mathbf{z}|\mathbf{y})$ in the table. The expressions for predicting and updating the Bernoulli estimates based on the potential information acquired by the sensor updates follow.

A. Prior

For a single track, which in the context of this paper is analogous to a Bernoulli, we write the hybrid state prior distribution as

$$f_{k-1}^{t}(\mathbf{y}) = f_{k-1}^{t}(\mathbf{x}|\tau, s)\xi_{k-1}^{t\tau}\mu_{k-1}^{t\tau s}o_{k-1}^{tv}, \tag{18}$$

while the prior existence probability is r_{k-1}^{t}. As mentioned above, we merge all the hypotheses of the previous time step, giving $w_{k-1}^{t} = 1$. The prior is a joint distribution over the continuous kinematic state and the discrete potential IDs, kinematic modes, and visibility states. In the following propositions, only the probability of the target being in the visible state is presented, i.e., o^{t1}, which we denote as η^{t}. The prior is decomposed into several states conditioned on the different discrete states. An example of the structure of a prior with two possible IDs and two possible kinematic modes is shown in Fig. 1. The expressions in the square boxes are not calculated themselves but can be constructed from the other expressions.

B. Prediction

All tracks are predicted from the previous time step $k-1$ to the current time step k. The predicted probabilities and densities are denoted by the subscript $(\cdot)_{k|k-1}$.

Proposition 1. *The prediction for the existence probability r^{t}, the visibility probability η^{t}, the ID probabilities $\xi^{t\tau}$, the mode probabilities $\mu^{t\tau s}$, and the kinematic density $f^{t}(\mathbf{x}|\tau, s)$ are done as*

$$r_{k|k-1}^{t} = r_{k-1}^{t}P_S(\Delta t), \tag{19}$$

$$\eta_{k|k-1}^{t} = (1 - \eta_{k-1}^{t})w^{01} + \eta_{k-1}^{t}w^{11}, \tag{20}$$

$$\xi_{k|k-1}^{t\tau} = \xi_{k-1}^{t\tau}, \tag{21}$$

$$\mu_{k|k-1}^{t\tau s} = \sum_{\bar{s}} \mu_{k-1}^{t\tau\bar{s}}\pi^{\bar{s}s}(\Delta t), \tag{22}$$

Table I
Nomenclature

$\mathbf{a}$	Association hypothesis
$b(\cdot)$	Birth intensity function
$1_{\Omega}(\cdot)$	Indicator function
$\mathbf{H}$	Measurement matrix
$\mathbf{H}^{*}$	Complementary measurement matrix
$\mathcal{N}(\cdot)$	Gaussian probability density function
μ	Mode probabilities
η	Probability of a target being visible
ξ	ID probabilities
$f(\cdot)$	Generic (single-target) probability density function (pdf)
$f_{\mathbf{y}}(\cdot)$	Transition density for hybrid state
$f_{\mathbf{z}}(\cdot)$	Measurement density conditional on hybrid state
$\mathbf{F}$	Process model transition matrix
$g[h]$	functional with test function
h	Generic hybrid state probability density function
j	Measurement index (superscript)
k	Time step index (subscript)
Δt	Interval between current and preceding time step
λ	Poisson intensity for false alarms
n	Number of tracks
o	Visibility probabilities
P_{S_c}	Constant survival probability
P_{D}	Detection probability
$\mathbf{P}_v$	Initial velocity covariance
π	Mode transition probabilities
$\mathbf{Q}$	Process noise covariance matrix
r	Existence probability
$\mathbf{R}$	Measurement noise covariance matrix
$\mathbf{R}_c$	Cartesian measurement noise covariance contribution
$\mathbf{R}_p$	Polar measurement noise covariance contribution
s	Model index (superscript)
τ	ID number (superscript)
t	Track index (superscript)
u	Poisson intensity of unknown targets
U	Unknown target intensity strength
v	Visibility state (superscript)
$\mathbf{v}$	Process noise
$\mathbf{w}$	Measurement noise
ω	Visibility transition probabilities *or* turn rate
Ω	Surveillance region
x	Kinematic (continuous) state vector
$\mathbf{y}$	Hybrid state vector
$\mathbf{z}$	Measurement vector
A	Target-provided (AIS) specific entity
R	Radar specific entity
$(\cdot)_k$	A (typically posterior) quantity at time step k
$(\cdot)_{k\|k-1}$	A predicted quantity at time step k
$\hat{(\cdot)}$	A Kalman filter estimate
$\tilde{(\cdot)}$	Latent variables that are marginalized away
$(\cdot)^{0}$	An initial quantity. Further meaning is context-dependent.
$(\cdot)_u$	Unknown target intensity parameter after convergence

Table II
Expressions for Creating, Updating, and Predicting the Bernoulli Components

	g	$h[1]$	$h(\mathbf{y})$
New target	λ	$u[P_D(\tilde{\mathbf{y}})f_{\mathbf{z}}(\mathbf{z}\|\tilde{\mathbf{y}})]$	$u(\mathbf{y})P_D(\mathbf{y})f_{\mathbf{z}}(\mathbf{z}\|\mathbf{y})$
Missed detection	$1-r^t_{k\|k-1}$	$r^t_{k\|k-1}f[1-P_D(\tilde{\mathbf{y}})]$	$r^t_{k\|k-1}f_{k\|k-1}(\mathbf{y})(1-P_D(\mathbf{y}))$
Detection	0	$r^t_{k\|k-1}f[P_D(\tilde{\mathbf{y}})f_{\mathbf{z}}(\mathbf{z}\|\tilde{\mathbf{y}})]$	$r^t_{k\|k-1}f^t_{k\|k-1}(\mathbf{y})P_D(\mathbf{y})f_{\mathbf{z}}(\mathbf{z}\|\mathbf{y})$
Prediction	$1-r^t_{k-1}f[P_S(\tilde{\mathbf{y}})]$	$r^t_{k-1}f[P_S(\tilde{\mathbf{y}})]$	$r^t_{k-1}\int f^t_{k\|k-1}(\mathbf{y}\|\tilde{\mathbf{y}})P_S(\tilde{\mathbf{y}})f_{k-1}(\tilde{\mathbf{y}}))\mathrm{d}\tilde{\mathbf{y}}$

$$f^t_{k|k-1}(\mathbf{x}|\tau,s)=\int f_{\mathbf{y}}(\mathbf{x}|\tau,s,\tilde{\mathbf{x}})f^t_{k-1}(\tilde{\mathbf{x}}|\tau,s)\mathrm{d}\tilde{\mathbf{x}}, \tag{23}$$

where

$$f^t_{k-1}(\tilde{\mathbf{x}}|\tau,s)=\sum_{\tilde{s}}\frac{\mu^{t\tau\tilde{s}}_{k-1}\pi^{\tilde{s}s}f^t_{k-1}(\tilde{\mathbf{x}}|\tau,\tilde{s})}{\sum_{\tilde{s}}\mu^{t\tau\tilde{s}}_{k-1}\pi^{\tilde{s}s}(\Delta t)}. \tag{24}$$

Proof. The proof builds upon [7], but is modified to also account for the inclusion of the IDs in the state vector. It should be noted that the survival probability is only dependent on the times of the measurements' arrival, which are independent of the state. Because the IDs are assumed to be static the transition model for the IDs becomes a Kronecker delta $\delta_{\tau\tilde{\tau}}$. It is defined as

$$\delta_{\tau\tilde{\tau}}=\begin{cases}1 & \text{if } \tau=\tilde{\tau}\\ 0 & \text{if } \tau\neq\tilde{\tau}\end{cases}. \tag{25}$$

First, we write out $h(\mathbf{y})$ from Table II:

$$\begin{aligned}h(\mathbf{y})&=r^t_{k-1}\int f^t_{k|k-1}(\mathbf{y}|\tilde{\mathbf{y}})P_S(\tilde{\mathbf{y}})f_{k-1}(\tilde{\mathbf{y}})\mathrm{d}\tilde{\mathbf{y}}\\&=r^t_{k-1}P_S(\Delta t)\Big(\sum_{\tilde{v}}f(\tilde{v})f(v|\tilde{v})\Big)\times\\&\quad\times\sum_{\tilde{\tau}}f_{k-1}(\tilde{\tau})\delta_{\tau\tilde{\tau}}\sum_{\tilde{s}}f_{k-1}(\tilde{s}|\tilde{\tau})f^t_{k|k-1}(s|\tilde{s})\times\\&\quad\times\int f^t_{k|k-1}(\mathbf{x}|s,\tau,\tilde{\mathbf{x}})f_{k-1}(\tilde{\mathbf{x}}|\tilde{s},\tilde{\tau})\mathrm{d}\tilde{\mathbf{x}}\\&=r^t_{k-1}P_S(\Delta t)\Big(\sum_{\tilde{v}}f(\tilde{v})f(v|\tilde{v})\Big)f_{k-1}(\tau)\times\\&\quad\times\sum_{\tilde{s}}f_{k-1}(\tilde{s}|\tau)f^t_{k|k-1}(s|\tilde{s})\int f^t_{k|k-1}(\mathbf{x}|s,\tau,\tilde{\mathbf{x}})\times\\&\quad\times f_{k-1}(\tilde{\mathbf{x}}|\tilde{s},\tau)\mathrm{d}\tilde{\mathbf{x}}\\&=r^t_{k-1}P_S(\Delta t)\Big(\sum_{\tilde{v}}o^{t\tilde{v}}_{k-1}w^{\tilde{v}v}\Big)\xi^{t\tau}_{k-1}\sum_{\tilde{s}}\mu^{\tau s}_{k-1}\pi^{\tilde{s}s}(\Delta t)\times\\&\quad\times\int f^{t\tau s}_{k|k-1}(\mathbf{x}|s,\tau,\tilde{\mathbf{x}})f_{k-1}(\tilde{\mathbf{x}}|\tilde{s},\tau)\mathrm{d}\tilde{\mathbf{x}},\end{aligned} \tag{26}$$

which uses the fact that only the conditioning on the most recent variable is relevant. Marginalizing this, one gets

$$\begin{aligned}h(s,\tau)&=r^t_{k-1}\int\sum_{v}h(\mathbf{x},s,\tau,v)\mathrm{d}\mathbf{x}\\&=r^t_{k-1}P_S(\Delta t)\xi^{t\tau}_{k-1}\sum_{\tilde{s}}\mu^{t\tau\tilde{s}}_{k-1}\pi^{\tilde{s}s}(\Delta t),\end{aligned} \tag{27}$$

$$h(\tau)=r^t_{k-1}\sum_{s}h(s,\tau)=P_S(\Delta t)\xi^{t\tau}_{k-1}, \tag{28}$$

$$\begin{aligned}h(v)&=r^t_{k-1}\int\sum_{\tau}\sum_{s}h(\mathbf{x},s,\tau,v)\mathrm{d}\mathbf{x}\\&=r^t_{k-1}P_S(\Delta t)\Big(\sum_{\tilde{v}}o^{t\tilde{v}}_{k-1}w^{\tilde{v}v}\Big)\end{aligned} \tag{29}$$

$$h[1]=r^t_{k-1}\sum_{\tau}h(\tau)=r^t_{k-1}P_S(\Delta t). \tag{30}$$

Inserting this in (14)–(17) provides the expressions for the hybrid states. Note that the expression for the visibility probability $\eta^t_{k|k-1}$ follows from the fact that $o^{t0}_{k-1}=1-o^{t1}_{k-1}=1-\eta^t_{k-1}$. The expression for the existence probability $r^t_{k|k-1}$ is found by inserting $g(\mathbf{y})=r^t_{k-1}P_S(\Delta t)$ from Table II and $h[1]$ into (11). □

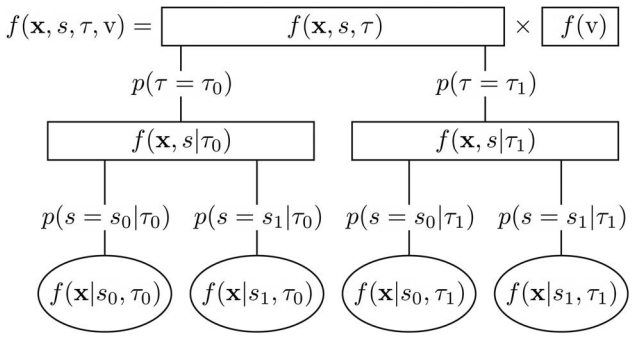

Fig. 1. The structure of the distribution of a hybrid state with two kinematic modes and two possible IDs.

C. Posterior

The individual posterior distributions, conditioned on either a detection or a missed detection, are calculated after the prediction. The four possibilities for a track when new measurements arrive are

- The previously unknown track is detected for the first time.
- The previously detected track is detected again.
- The previously detected track is not detected.
- The previously unknown track is not detected.

Any tracks covered by the fourth alternative will be represented by the unknown target density, and do not need to be considered specifically. The posterior distributions for the three first possibilities are presented in the following propositions.

Proposition 2. *Initialization of a new track on a measurement indexed by j is done as*

$$w_k^{tj} = \begin{cases} \lambda + cUP_D\eta^0 & \text{for radar} \\ cU\sum_{\tilde{\tau}} \xi_u^{\tilde{\tau}} f_\tau(\tau^j|\tilde{\tau}) & \text{for target-provided} \end{cases}, \quad (31)$$

$$r_k^{tj} = \begin{cases} \dfrac{UP_D\eta^0}{\lambda + UP_D\eta^0} & \text{for radar} \\ 1 & \text{for target-provided} \end{cases}, \quad (32)$$

$$\eta_k^{tj} = \begin{cases} 1 & \text{for radar} \\ \eta_u & \text{for target-provided} \end{cases}, \quad (33)$$

$$\xi_k^{t\tau j} = \begin{cases} \xi_u^\tau & \text{for radar} \\ f_\tau(\tau^{\mathbf{z}}|\tau) & \text{for target-provided} \end{cases}, \quad (34)$$

$$\mu_k^{t\tau s j} = \mu_u^s, \quad (35)$$

$$f_k^{tj}(\mathbf{x}|s,\tau) = f_{\mathbf{z}}(\mathbf{z}|\mathbf{x},s,\tau) f_u(\mathbf{x})/c, \quad (36)$$

where $c = \int f_{\mathbf{z}}(\mathbf{z}|\mathbf{x},s,\tau) f_u(\mathbf{x})\mathrm{d}\mathbf{x}$ is a constant.

Proof. Firstly, for radar measurements, we have that

$$h(\mathbf{y}) = UP_D(v) o_u^v \xi_u^\tau \mu_u^{\tau s} f_u(\mathbf{x}) f_{\mathbf{z}}(\mathbf{z}|\mathbf{x},s,\tau), \quad (37)$$

which follows from (2) and Table II. Furthermore,

$$h(s,\tau,v) = cUP_D(v) o_u^v \xi_u^\tau \mu_u^{\tau s}, \quad (38)$$

$$h(\tau,v) = cUP_D(v) o_u^v \xi_u^\tau, \quad (39)$$

$$h(v) = cUP_D(v) o_u^v, \quad (40)$$

$$h[1] = cUP_D\eta^0, \quad (41)$$

where c is a constant resulting from the marginalization over $\mathbf{x}$.

For target-provided measurements, we have that $f_{\mathbf{z}}(\mathbf{z}|\mathbf{x},s,\tau) = f_{\mathbf{p}}(\mathbf{p}|\mathbf{x},s,\tau) f_\tau(\tau^{\mathbf{z}}|\tau)$. This means that

$$h(\mathbf{y}) = U o_u^v \xi_u^\tau \mu_u^{\tau s} f_\tau(\tau^{\mathbf{z}}|\tau) f_u(\mathbf{x}) f_{\mathbf{z}}(\mathbf{p}|\mathbf{x},s,\tau). \quad (42)$$

The probability of detection is omitted here, as it is defined as 1 whenever a target-provided measurement has been received. Furthermore,

$$h(s,\tau,v) = cU o_u^v \xi_u^\tau \mu_u^{\tau s} f_\tau(\tau^{\mathbf{z}}|\tau), \quad (43)$$

$$h(\tau) = cU \xi_u^\tau f_\tau(\tau^{\mathbf{z}}|\tau), \quad (44)$$

$$h(v) = cU o_u^v \textstyle\sum_{\tilde{\tau}} \xi_u^{\tilde{\tau}} f_\tau(\tau^{\mathbf{z}}|\tilde{\tau}), \quad (45)$$

$$h[1] = cU \textstyle\sum_{\tilde{\tau}} \xi_u^{\tilde{\tau}} f_\tau(\tau^{\mathbf{z}}|\tilde{\tau}), \quad (46)$$

where c again is a constant.

Inserting these expressions in (14)–(17) give (33)–(36), i.e., the distributions of the individual hybrid states of a new target. Furthermore, we have from Table II that g is the clutter density, which is λ for radar measurements, and 0 for target-provided measurements. We insert g and $h[1]$ in (10) and (11) to get (31) and (32). The expression for the ID probability in the event of initialization on a transmitted measurement requires some further explanation. Keeping in mind the prior distribution for the IDs (4), we have that

$$\begin{aligned} \xi_k^{t\tau j} &= \frac{h(\tau)}{h[1]} \\ &= \frac{\xi_u^\tau f_\tau(\tau^{\mathbf{z}}|\tau)}{\sum_{\tilde{\tau}} \xi_u^{\tilde{\tau}} f_\tau(\tau^{\mathbf{z}}|\tilde{\tau})} \\ &= \begin{cases} \dfrac{f_\tau(\tau^{\mathbf{z}}|\tau)(1-\xi_u^0)/|\mathcal{V}-1|}{\sum_{\tilde{\tau}} f_\tau(\tau^{\mathbf{z}}|\tilde{\tau})(1-\xi_u^0)/|\mathcal{V}-1|} & \text{if } \tau > 0 \\ 0 & \text{if } \tau = 0 \end{cases} \\ &= \begin{cases} \dfrac{f_\tau(\tau^{\mathbf{z}}|\tau)}{\sum_{\tilde{\tau}} f_\tau(\tau^{\mathbf{z}}|\tilde{\tau})} & \text{if } \tau > 0 \\ 0 & \text{if } \tau = 0 \end{cases} \\ &= \begin{cases} f_\tau(\tau^{\mathbf{z}}|\tau) & \text{if } \tau > 0 \\ 0 & \text{if } \tau = 0 \end{cases} = f_\tau(\tau^{\mathbf{z}}|\tau), \end{aligned} \quad (47)$$

where we have used that $\sum_{\tilde{\tau}} f_\tau(\tau^{\mathbf{z}}|\tilde{\tau}) = 1$. If a different prior distribution than (4) is used for the IDs, it can be accommodated by replacing the final expression with the one in the second line of the above expression. □

Proposition 3. *Updating based on a missed detection is done as*

$$w_k^{t0} = \begin{cases} 1 - r_{k|k-1}^t \eta_{k|k-1}^t P_D & \text{for radar} \\ 1 & \text{for target-provided} \end{cases}, \quad (48)$$

$$r_k^{t0} = \begin{cases} \dfrac{r_{k|k-1}^t (1 - \eta_{k|k-1}^t P_D)}{1 - r_{k|k-1}^t \eta_{k|k-1}^t P_D} & \text{for radar} \\ r_{k|k-1}^t & \text{for target-provided} \end{cases}, \quad (49)$$

$$\eta_k^{t0} = \begin{cases} \dfrac{(1-P_D)\eta_{k|k-1}^t}{1 - P_D \eta_{k|k-1}^t} & \text{for radar} \\ \eta_{k|k-1}^t & \text{for target-provided} \end{cases}, \quad (50)$$

$$\xi_k^{t\tau 0} = f_{k|k-1}^t(\tau), \quad (51)$$

$$\mu_k^{t\tau s 0} = f_{k|k-1}^t(s|\tau), \quad (52)$$

$$f_k^{t0}(\mathbf{x}|\tau,s) = f_{k|k-1}^t(\mathbf{x}|\tau,s). \quad (53)$$

Remark 2. The inclusion of target-provided measurement types in the case of a missed detection is somewhat artificial. The expressions are the same as for the prediction, as the absence of target-provided measurements gives no additional information to the tracking

algorithm. This follows from the definition of the detection probability in Section III, i.e., that $P_D = 0$ for target-provided measurements when they have not been received. For later use, the expressions are nevertheless written out here.

Proof. We have that

$$h(\mathbf{y}) = r^t_{k|k-1}(1 - P_D(v))o^{tv}_{k|k-1}\xi^{t\tau}_{k|k-1}\mu^{t\tau s}_{k|k-1} f_{k|k-1}(\mathbf{x}|s,\tau), \tag{54}$$

where the corresponding expression from Table II has been written out. Similarly, as to what was done previously, we find through marginalization that

$$\begin{aligned} h(s,\tau,v) &= r^t_{k|k-1}(1 - P_D(v))o^{tv}_{k|k-1}\xi^{t\tau}_{k|k-1}\mu^{t\tau s}_{k|k-1} \\ h(\tau,v) &= r^t_{k|k-1}(1 - P_D(v))o^{tv}_{k|k-1}\xi^{t\tau}_{k|k-1} \\ h(v) &= r^t_{k|k-1}(1 - P_D(v))o^{tv}_{k|k-1}. \end{aligned} \tag{55}$$

Again, the different detection probabilities have to be taken into account when summing over the visibility states, giving

$$\begin{aligned} h[1] &= r^t_{k|k-1}((1 - P_D)\eta^t_{k|k-1} + (1 - \eta^t_{k|k-1})) \\ &= r^t_{k|k-1}(1 - P_D\eta^t_{k|k-1}) \end{aligned} \tag{56}$$

for radar updates and $h[1] = 1$ for AIS updates. Inserting this in (14)–(17) gives the wanted expressions for the hybrid states. Furthermore, we get from Table II that g is given by $1 - r^t_{k|k-1}$, which together with $h[1]$ gives us (48) and (49) by using (10) and (11). □

Proposition 4. *Updating based on a detection is done as*

$$w^{tj}_k = \begin{cases} P_D\eta^t_{k|k-1}r^t_{k|k-1}\sum_{\tilde{\tau}}\xi^{t\tilde{\tau}}_{k|k-1}\sum_{\tilde{s}}\mu^{t\tilde{\tau}\tilde{s}}_{k|k-1}l^{t\tilde{\tau}\tilde{s}j} \\ \quad \textit{for radar} \\ r^t_{k|k-1}\sum_{\tilde{\tau}}\xi^{t\tilde{\tau}}_{k|k-1}\sum_{\tilde{s}}\mu^{t\tilde{\tau}\tilde{s}}_{k|k-1}l^{t\tilde{\tau}\tilde{s}j} \\ \quad \textit{for target-provided} \end{cases}, \tag{57}$$

$$r^{tj}_k = 1, \tag{58}$$

$$\eta^{tj}_k = \begin{cases} 1 & \textit{for radar} \\ \eta^t_{k|k-1} & \textit{for target-provided} \end{cases}, \tag{59}$$

$$\xi^{t\tau j}_k = \frac{\xi^{t\tau}_{k|k-1}\sum_{\tilde{s}}l^{t\tau\tilde{s}j}}{\sum_{\tilde{\tau}}\xi^{t\tilde{\tau}}_{k|k-1}\sum_{\tilde{s}}l^{t\tilde{\tau}\tilde{s}j}}, \tag{60}$$

$$\mu^{t\tau sj}_k = \frac{\mu^{t\tau s}_{k|k-1}l^{t\tau sj}}{\sum_{\tilde{s}}\mu^{t\tau\tilde{s}}_{k|k-1}l^{t\tau\tilde{s}j}}, \tag{61}$$

$$f^{tj}_k(\mathbf{x}|\tau,s) = \frac{f_{\mathbf{z}}(\mathbf{z}|\mathbf{x},\tau,s)f^t_{k|k-1}(\mathbf{x}|\tau,s)}{l^{t\tau sj}}, \tag{62}$$

where

$$l^{t\tau sj} = f_\tau(\tau^j|\tau)\int f_{\mathbf{z}}(\mathbf{z}^j_k|\tilde{\mathbf{x}})f^{t\tau s}_{k|k-1}(\tilde{\mathbf{x}})\mathrm{d}\tilde{\mathbf{x}} \tag{63}$$

for target-provided measurements and

$$l^{t\tau sj} = \int f_{\mathbf{z}}(\mathbf{z}^j_k|\tilde{\mathbf{x}})f^{t\tau s}_{k|k-1}(\tilde{\mathbf{x}})\mathrm{d}\tilde{\mathbf{x}} \tag{64}$$

for radar measurements.

Proof. Writing out the expression for a detection in Table II, we have that

$$\begin{aligned} h(\mathbf{y}) = r^t_{k|k-1}P_D(v)o^{tv}_{k|k-1}\xi^{t\tau}_{k|k-1}\mu^{t\tau s}_{k|k-1}\times \\ \times f^{t\tau s}_{k|k-1}(\mathbf{x})f_{\mathbf{z}}(\mathbf{z}|\mathbf{x},s,\tau), \end{aligned} \tag{65}$$

which we marginalize to obtain

$$\begin{aligned} h(s,\tau,v) &= r^t_{k|k-1}P_D(v)o^{tv}_{k|k-1}\xi^{t\tau}_{k|k-1}\mu^{t\tau s}_{k|k-1}l^{t\tau sj} \\ h(\tau,v) &= r^t_{k|k-1}P_D(v)o^{tv}_{k|k-1}\xi^{t\tau}_{k|k-1}\sum_s\mu^{t\tau s}_{k|k-1}l^{t\tau sj} \\ h(v) &= r^t_{k|k-1}P_D(v)o^{tv}_{k|k-1}\sum_\tau\xi^{t\tau}_{k|k-1}\sum_s\mu^{t\tau s}_{k|k-1}l^{t\tau sj}. \end{aligned} \tag{66}$$

For radar, we have that $P_D(v = 1) = P_D$ and 0 otherwise, and for AIS $P_D(v) = P_D = 1$ if a measurement has been received. Using this, we get

$$h[1] = P_D\eta^t_{k|k-1}r^t_{k|k-1}\sum_\tau\xi^{t\tau}_{k|k-1}\sum_s\mu^{t\tau s}_{k|k-1}l^{t\tau sj} \tag{67}$$

for radar updates and

$$h[1] = r^t_{k|k-1}\sum_\tau\xi^{t\tau}_{k|k-1}\sum_s\mu^{t\tau s}_{k|k-1}l^{t\tau sj} \tag{68}$$

for AIS updates. The expressions for the hybrid states result from inserting this in (14)–(17). We see from Table II that $g = 0$, and using this together with $h[1]$, we get (57) and (58) from (10) and (11). □

D. Mixture Reduction

The mixture reduction is done similarly to what is done in the JIPDA. That is, all the association hypotheses for each track are merged. An association hypothesis $\mathbf{a}_k$ from the set of all possible association hypotheses $\mathcal{A}_k$ contains individual track-to-measurement associations a^t. The probabilities for the individual association hypotheses are

$$\Pr(\mathbf{a}_k) \propto \prod_{t\ s.t\ a^t=0} w^{ta^t}_k \prod_{t\ s.t\ a^t>0} w^{ta^t}_k/\lambda, \tag{69}$$

where λ is the Poisson intensity for the false alarms, and the fact that $\sum_{\mathbf{a}_k\in\mathcal{A}_k}\Pr(\mathbf{a}_k) = 1$ is used to normalize the probabilities. This in turn provides the marginal probabilities for the associations as

$$p^{tj}_k = \sum_{\mathbf{a}_k\ s.t.\ a^t=j}\Pr(\mathbf{a}_k). \tag{70}$$

The mixture reduction remains the same irrespective of the type of measurement, as all differences are handled during the calculation of the individual posterior distributions.

Proposition 5. *We have that*

$$r_k^t = \sum_{j=0}^{m_k} r_k^{tj} p^{tj}, \tag{71}$$

$$\eta_k^t = \sum_{j=0}^{m_k} \underbrace{\frac{1}{r_k^t} r_k^{tj} p_k^{tj}}_{\beta_k^{tj}} \eta_k^{tj}, \tag{72}$$

$$\xi_k^{t\tau} = \sum_{j=0}^{m_k} \underbrace{\frac{1}{r_k^t} r_k^{tj} p_k^{tj}}_{\beta_k^{tj}} \xi_k^{t\tau j}, \tag{73}$$

$$\mu_k^{t\tau s} = \sum_{j=0}^{m_k} \underbrace{\frac{1}{\xi_k^{t\tau} r_k^t} \xi_k^{t\tau j} r_k^{tj} p_k^{tj}}_{\beta_k^{t\tau j}} \mu_k^{t\tau s j}, \tag{74}$$

$$f_k^{t\tau s}(\mathbf{x}) = \sum_{j=0}^{m} \underbrace{\frac{\mu_k^{t\tau s j} \xi_k^{t\tau j} r_k^{tj} p_k^{tj}}{\mu_k^{t\tau s} \xi_k^{t\tau} r_k^t}}_{\beta^{t\tau s j}} f_{k_i}^{t\tau s j}(\mathbf{x}), \tag{75}$$

where

$$\beta_k^{tj} = \frac{r_k^{tj} p_k^{tj}}{r_k^t} = \begin{cases} \dfrac{p_k^{tj}}{r_k^t}, & j > 0 \\ \dfrac{r_k^0 p_k^{t0}}{r_k^t}, & j = 0 \end{cases}, \tag{76}$$

$$\beta_k^{t\tau j} = \frac{\xi_k^{t\tau j} r_k^{tj} p_k^{tj}}{\xi_k^{t\tau} r_k^t} = \beta_k^{tj} \frac{\xi_k^{t\tau j}}{\xi_k^{t\tau}}, \tag{77}$$

$$\beta_k^{t\tau s j} = \frac{\mu_k^{t\tau s j} \xi_k^{t\tau j} r_k^{tj} p_k^{tj}}{\mu_k^{t\tau s} \xi_k^{t\tau} r_k^t} = \beta_k^{t\tau j} \frac{\mu_k^{t\tau s j}}{\mu_k^{t\tau s}}. \tag{78}$$

Using the individual $f_k^{t\tau s j}(\mathbf{x})$, the combined state $f_k^{t\tau s}(\mathbf{x})$ can be approximated by use of moment matching techniques.

Proof. The MBM containing the posterior track estimates, weights, and existence probabilities can be approximated as a multi-Bernoulli. A thorough proof of this, and more context regarding the MBM, can be found in [34]. Drawing from the aforementioned proof, in combination with the proof in [7, Appendix D], we have that the posterior distribution over $\mathbf{y}$ can be approximated as

$$f_k^t(\mathbf{y}) \approx \sum_{j=1}^{m_k} \beta_k^{tj} f_k^{tj}(\mathbf{y}) \tag{79}$$

where

$$\beta_k^{tj} = \frac{r_k^{tj} p_k^{tj}}{r_k^t} \tag{80}$$

and

$$f_k^{tj}(\mathbf{y}) = o_k^{tvj} \xi_k^{t\tau j} \mu_k^{t\tau s j} f_k^{ts\tau j}(\mathbf{x}). \tag{81}$$

Using this, together with the approximation that the visibility is independent of the other states, we can write

$$\begin{aligned}
&\sum_{j=1}^{m_k} \beta_k^{tj} f_k^{tj}(\mathbf{y}) \approx \sum_{j=1}^{m_k} \beta_k^{tj} \xi_k^{t\tau j} \mu_k^{t\tau s j} f_k^{ts\tau j}(\mathbf{x}) \sum_{j=1}^{m_k} \beta_k^{tj} o_k^{tvj} \\
&= \frac{\sum_{j=1}^{m_k} \beta_k^{tj} \xi_k^{t\tau j} \mu_k^{t\tau s j} f_k^{ts\tau j}(\mathbf{x})}{\sum_{j=1}^{m_k} \beta_k^{tj} \xi_k^{t\tau j} \mu_k^{t\tau s j}} \frac{\sum_{j=1}^{m_k} \beta_k^{tj} \xi_k^{t\tau j} \mu_k^{t\tau s j}}{\sum_{j=1}^{m_k} \beta_k^{tj} \xi_k^{t\tau j}} \times \\
&\quad \times \sum_{j=1}^{m_k} \beta_k^{tj} \xi_k^{t\tau j} \sum_{j=1}^{m_k} \beta_k^{tj} o_k^{tvj} \\
&= \sum_{j=1}^{m_k} \frac{\beta_k^{tj} \xi_k^{t\tau j} \mu_k^{t\tau s j}}{\sum_{j=1}^{m_k} \beta_k^{tj} \xi_k^{t\tau j} \mu_k^{t\tau s j}} f_k^{ts\tau j}(\mathbf{x}) \sum_{j=1}^{m_k} \frac{\beta_k^{tj} \xi_k^{t\tau j}}{\sum_{j=1}^{m_k} \beta_k^{tj} \xi_k^{t\tau j}} \mu_k^{t\tau s j} \times \\
&\quad \times \sum_{j=1}^{m_k} \beta_k^{tj} \xi_k^{t\tau j} \sum_{j=1}^{m_k} \beta_k^{tj} o_k^{tvj} \\
&= \underbrace{\sum_{j=1}^{m_k} \beta_k^{t\tau s j} f_k^{ts\tau j}(\mathbf{x})}_{f_k^{ts\tau}(\mathbf{x})} \underbrace{\sum_{j=1}^{m_k} \beta_k^{t\tau j} \mu_k^{t\tau s j}}_{\mu_k^{t\tau s}} \underbrace{\sum_{j=1}^{m_k} \beta_k^{tj} \xi_k^{t\tau j}}_{\xi_k^{t\tau}} \underbrace{\sum_{j=1}^{m_k} \beta_k^{tj} o_k^{tvj}}_{o_k^{tv}}.
\end{aligned} \tag{82}$$

Keeping in mind that $r_k^{tj} = 1 \,\forall\, j > 0$ and that $o_k^{t1j} = \eta_k^{tj} = 1 \,\forall\, j > 0$, we get the wanted expressions. Lastly, we get the expression for the existence probability r_k^t directly from [7]. □

VI. TARGET-PROVIDED MEASUREMENT HANDLING

The method shown in the previous section does not specify how the target-provided measurements are grouped before being sent to the tracker. In this section, we present three different ways of considering the target-provided measurements.

A. Method A: Sequential Measurement Processing

The first method for handling the incoming target-provided measurements is to process them, and perform the data association, as they arrive. This would mean that the predicting and updating of tracks is performed for each target-provided measurement, which can arrive at any time between radar measurement batches. This approach demands no further extensions to what is described above. The method is shown in Algorithm 1.

B. Method B: Precise Batch Measurement Processing

The second method performs the data association for the target-provided measurements at the times when radar measurements arrive. The method considers all the target-provided measurements that have arrived between the previous and current time steps as a batch of measurements. This method is conceptually similar to what is done in [13] and [17]. The method is shown

Algorithm 1 Method A: Sequential measurement processing

Require: target-provided measurements
$Z_A = \{\mathbf{z}_A^1, \ldots, \mathbf{z}_A^m\}$, radar measurements
$Z_R = \{\mathbf{z}_R^1, \ldots, \mathbf{z}_R^m\}$, tracks from previous time step
$X = \{\mathbf{x}^1, \ldots, \mathbf{x}^n\}$
for target-provided measurement $\mathbf{z}_A^j \in Z_A$ **do**
$X \leftarrow \text{PREDICT}(\mathrm{X}, \mathrm{t}_A^j)$ ▷ predict tracks to time of $\mathbf{z}_A^j$
$X \leftarrow \text{UPDATE}(\mathrm{X}, \mathbf{z}_A^j)$
end for
$X \leftarrow \text{PREDICT}(\mathrm{X}, \mathrm{t}_R)$ ▷ predict tracks to time of Z_R
$X \leftarrow \text{UPDATE}(\mathrm{X}, Z_R)$

in Algorithm 2. The target-provided measurements with the same ID are clustered together, and the data association is performed based on these clusters. The clustering means that the measurement likelihood has to be calculated for each cluster rather than for each measurement. The measurement likelihood for I_m measurements with the same ID is

$$f_{\mathbf{z}}(\mathbf{z}|\mathbf{x}) = f_{\mathbf{z}}(\mathbf{z}^1, \ldots, \mathbf{z}^{I_m}|\mathbf{x}) = \prod_{i=1}^{I_m} f_{\mathbf{z}}(\mathbf{z}^i|\mathbf{z}^{i-1}, \ldots, \mathbf{z}^1, \mathbf{x}), \tag{83}$$

where

$$f_{\mathbf{z}}(\mathbf{z}^i|\mathbf{z}^{i-1}, \ldots, \mathbf{z}^1, \mathbf{x}) = \int f_{\mathbf{z}}(\mathbf{z}^i|\mathbf{x}^i) f_{\mathbf{x}}(\mathbf{x}^i|\mathbf{z}^{i-1}, \ldots, \mathbf{z}^1, \mathbf{x}) \mathrm{d}\mathbf{x}^i. \tag{84}$$

This has to be calculated for each measurement that has arrived between the radar updates. The measurements are sorted according to their time stamp, with $\mathbf{z}^{I_m}$ being the most recent measurement. This expression effectively replaces the integral in (63). The individual kinematic states are calculated as

$$f_k^{t\tau s j}(\mathbf{x}|\mathbf{z}^i, \mathbf{z}^{i-1}, \ldots, \mathbf{z}^1, \mathbf{x}) = \frac{f_{\mathbf{z}}(\mathbf{z}^i|\mathbf{x}^i) f_{\mathbf{x}}(\mathbf{x}^i|\mathbf{z}^{i-1}, \ldots, \mathbf{z}^1, \mathbf{x})}{\int f_{\mathbf{z}}(\mathbf{z}^i|\mathbf{x}^i) f_{\mathbf{x}}(\mathbf{x}^i|\mathbf{z}^{i-1}, \ldots, \mathbf{z}^1, \mathbf{x}) \mathrm{d}\mathbf{x}^i}. \tag{85}$$

This expression can be calculated using, e.g., a Kalman filter. A thorough explanation of this recursive measurement likelihood calculation can be found in the supplementary material of [13]. With these expressions established, the other calculations and expressions are identical to Method A.

C. Method C: Batch Measurement Processing With Added Noise

In Section III, it is assumed that the radar measurements of a single measurement batch are synchronized, i.e., they all arrive at the same time. We do not make the same assumption for the target-provided measurements. However, making this assumption would allow us to simplify the handling of the measurements and remove some of the computational complexity of the above methods. Such an approach would be well suited when the radar frequency is high, as the timing errors would be small. Algorithm 3 describes the approach. Furthermore, only the most recent measurement is considered when a target has transmitted more than one measurement between radar updates. In addition, this method should be used with a higher measurement noise level to account for the synchronization errors.

Algorithm 2 Method B: Precise batch measurement processing

Require: target-provided measurement clusters
$Z_A = \{\mathbf{z}_A^1, \ldots, \mathbf{z}_A^m\}$, radar measurements
$Z_R = \{\mathbf{z}_R^1, \ldots, \mathbf{z}_R^m\}$, tracks from previous time step
$X = \{\mathbf{x}^1, \ldots, \mathbf{x}^n\}$
for track $\mathbf{x}^t \in X$ **do**
for target-provided measurement cluster $\mathbf{z}_A^j \in Z_A$ **do**
$\mathbf{x}^{t,j} \leftarrow \text{COPY}(\mathbf{x}^t)$
for target-provided measurement $\mathbf{z}^i \in \mathbf{z}_A^j$ **do**
$\mathbf{x}^{t,j} \leftarrow \text{PREDICT}(\mathbf{x}^t, \mathrm{t}_A^{j,i})$
$\mathbf{x}^{t,j} \leftarrow \text{UPDATE}(\mathbf{x}^j, \mathrm{t}_A^{j,i})$
end for
$l^{t,j} \leftarrow \text{MEASUREMENTLIKELIHOOD}(\mathbf{x}^{t,j}, \mathbf{z}_A^j)$
$\mathbf{x}^{t,j} \leftarrow \text{PREDICT}(\mathbf{x}^{t,j}, \mathrm{t}_R)$
end for
$X_{\text{new}}^{t,j} \leftarrow \mathbf{x}^{t,j}$
end for
$X \leftarrow \text{MIXTUREREDUCTION}(X_{\text{new}}, l)$
$X \leftarrow \text{UPDATE}(\mathrm{X}, Z_R)$

Algorithm 3 Method C: Batch measurement processing with added noise

Require: target-provided measurements
$Z_A = \{\mathbf{z}_A^1, \ldots, \mathbf{z}_A^m\}$, radar measurements
$Z_R = \{\mathbf{z}_R^1, \ldots, \mathbf{z}_R^m\}$, tracks from previous time step
$X = \{\mathbf{x}^1, \ldots, \mathbf{x}^n\}$
$X \leftarrow \text{PREDICT}(\mathrm{X}, \mathrm{t}_R)$ ▷ predict tracks to time of Z_R, Z_A
$X \leftarrow \text{UPDATE}(\mathrm{X}, Z_A)$
$X \leftarrow \text{UPDATE}(\mathrm{X}, Z_R)$

Remark 3. When grouping the same-ID target-provided measurements, one has to keep in mind the assumption of only one measurement arising from each target. If a target transmits two target-provided measurements between radar updates, and one of the measurements has a corrupted ID number, then this would breach the assumption. The most obvious way to amend

this is to discard target-provided measurements whenever there are more measurements than tracks present. This will, however, interfere with initializing new tracks on the target-provided measurements. It should also be noted that if the radar frequency is higher than the target-provided measurement transmission frequency, a cluster will always only contain a single measurement. This would avoid the aforementioned problem and simplify calculations.

Remark 4. When using (83), the discrete hybrid states will take their most likely value as a mean over the information from the measurements in the cluster. This is as opposed to obtaining the most likely value at the most recent target-provided measurement. This could theoretically impact the estimation of the discrete states. For example, if two measurements in a cluster indicate two different kinematic models, then this disparity will not be captured when using the batch processing methods.

VII. IMPLEMENTATION

A. Utilization of Gaussian-Linearity

To make the implementation tractable, we model the individual kinematic states and the measurement likelihoods as Gaussian distributions. This allows us to use an Extended Kalman Filter when predicting and updating the kinematic estimates. The measurement likelihoods are defined as

$$f_{\mathbf{z}}^{R}(\mathbf{z}_k|\mathbf{y}_k) = \mathcal{N}(\mathbf{z}_k|\mathbf{H}_R\mathbf{x}, \mathbf{R}_R) \tag{86}$$

for radar measurements and as

$$f_{\mathbf{p}}(\mathbf{p}_k|\mathbf{y}_k) = \mathcal{N}(\mathbf{p}_k|\mathbf{H}_A\mathbf{x}, \mathbf{R}_A) \tag{87}$$

for the positional part of the AIS measurements. Furthermore, the kinematic transition density $f_{\mathbf{x}}^{s\tau}(\mathbf{x}_k|\mathbf{x}_{k-1})$ is assumed to be in the form of a Gaussian

$$f_{\mathbf{x}}^{s\tau}(\mathbf{x}_k|\mathbf{x}_{k-1}) = \mathcal{N}(\mathbf{x}_k|\mathbf{f}^{(s)}(\mathbf{x}_{k-1}), \mathbf{Q}^{(s)}). \tag{88}$$

The transition model is linearized when needed to enable EKF prediction and Gaussian moment matching for mixture reduction.

The kinematic unknown target density from (2) is defined as

$$f_u(\mathbf{x}) = 1_\Omega(\mathbf{H}^{(s)}\mathbf{x})\mathcal{N}(\mathbf{H}^{*(s)}\mathbf{x}; \mathbf{0}, \mathbf{P}_v), \tag{89}$$

where $1_\Omega(\cdot)$ is an indicator function, which is 1 when the unknown target is within the surveillance area, and $\mathbf{H}^{*(s)}$ is the permutation matrix corresponding to the nonpositional states of the state vector $\mathbf{x}$. Using this, we have that

$$\begin{aligned} &f_{\mathbf{z}}(\mathbf{z}|\mathbf{x}, s, \tau) f_u(\mathbf{x}) \\ &= 1_\Omega(\mathbf{H}^{(s)}\mathbf{x})\mathcal{N}(\mathbf{z}_k^{at}|\mathbf{H}^{(s)}\mathbf{x}, \mathbf{R}^s)\mathcal{N}(\mathbf{H}^{*(s)}\mathbf{x}|\mathbf{0}, \mathbf{P}_v^{(s)}). \end{aligned} \tag{90}$$

In the case of a large enough surveillance area Ω, and under the assumption of Gaussian-linearity, this can be approximated as $\mathcal{N}(\mathbf{x}|\hat{\mathbf{x}}_0^s, \mathbf{P}_0^s)$. Furthermore, this means that the constant c in Proposition 2 becomes

$$c = \int f_{\mathbf{z}}(\mathbf{z}|\mathbf{x}, s, \tau) f_u(\mathbf{x}) \mathrm{d}\mathbf{x} \approx \int \mathcal{N}(\mathbf{x}|\hat{\mathbf{x}}_0^s, \mathbf{P}_0^s) \mathrm{d}\mathbf{x} = 1. \tag{91}$$

A more thorough proof regarding the unknown target density can be found in Appendix C of [7].

B. Gating

Because the target-provided measurements can arrive at any time, the number of times we have to perform gating increases considerably. The main computational cost of this is the number of predictions. Thus, we should consider this when creating the gating procedure.

Several different gating methods are presented in [33]. The first method relies on gating for each kinematic model, and it uses all measurements that have been gated by any of the models. A different method is a centralized gating procedure, which makes an approximation across all models using a single gate. We use a somewhat more refined method, the Two-Step Model Probability Weighted Gating (TS-MPWG) method. TS-MPWG was also presented in [33]. The first step in the method is a centralized gating procedure

$$f_{k|k-1}^{t}(\mathbf{x}) = \sum_{\tilde{\tau}} \xi_{k|k-1}^{t\tilde{\tau}} \sum_{\tilde{s}} \mu_{k|k-1}^{t\tilde{\tau}\tilde{s}} f_{k|k-1}^{t\tilde{\tau}\tilde{s}}(\mathbf{x}), \tag{92}$$

where $f_{k|k-1}^{t}(\mathbf{x}) = \mathcal{N}(\mathbf{x}|\hat{\mathbf{x}}_{k|k-1}, \hat{\mathbf{P}}_{k|k-1})$ provides the gate center $\hat{\mathbf{x}}_{k|k-1}$ and the predicted covariance $\hat{\mathbf{P}}_{k|k-1}$. Furthermore, the innovation covariance becomes

$$\mathbf{S} = \mathbf{H}\hat{\mathbf{P}}_{k|k-1}\mathbf{H}^\top + \mathbf{R}_k. \tag{93}$$

If no measurements are gated during the first step, then the next step is initiated. Here, the gate is determined by the largest possible model error and should encompass any measurements generated by the target even if the chosen kinematic model is wrong. Thus, the TS-MPWG method can exploit the more computationally effective nature of the central gating method while compensating for eventual model errors. Adapting the expressions in [33] to this model, the gate in the second step is determined by the maximal difference between $\hat{\mathbf{x}}_{k|k-1}$ and the individual $\hat{\mathbf{x}}_{k|k-1}^{t\tau s}$. This error is

$$K_{\max} = \arg\max_{\tau,s} \|\mathbf{H}\hat{\mathbf{x}}_{k|k-1} - \mathbf{H}\hat{\mathbf{x}}_{k|k-1}^{t\tau s}\|^2. \tag{94}$$

Using this, we calculate the gate volume as

$$\mathbf{S}_d = \mathbf{S} + \mathbf{K}_{\max} \tag{95}$$

where

$$\mathbf{K}_{\max} = \mathrm{diag}[\overbrace{K_{\max}, \ldots, K_{\max}}^{n}] \tag{96}$$

for a measurement space of dimension n.

Furthermore, it would be beneficial to have the possibility of gating target-provided measurements between two radar time steps without having to predict the state

of all tracks. We can achieve this by utilizing one of the methods described in [36]. The method involves expanding the gate size according to a fixed presumed maximum velocity. That is, rather than predicting the track from time t_{k-1} to t_k, the gate accounts for movement in all directions at a very high speed. This method gives very large validation gates, and we only use it as a preliminary step before using the TS-MPWG method. Here, the radius of the gate is decided by

$$r_k = 2r_{k_0} + (t_k - t_{k-1})v_{\max} \tag{97}$$

where $v_{\max}$ is a parameter representing the largest possible speed for a target, and

$$r_{k_0} = \sqrt{\gamma_G \text{eig}(\mathbf{R})_{\max}}. \tag{98}$$

Here, γ is the gate size, and $\text{eig}(\mathbf{R})_{\max}$ is the largest eigenvalue of the measurement covariance matrix.

C. Initialization and Termination

Due to target-provided measurements never being clutter measurements, care should be taken when choosing the initialization scheme. In JIPDA tracking algorithms, new tracks are usually only initialized on so-called free measurements, i.e., measurements that have not been gated by any tracks at the current time step. When using this scheme, a target-provided measurement belonging to an uninitialized target, which falls within the validation gate of a previously initialized target, would most likely assign the measurement to the previously initialized target. However, a scheme that initiates tracks on all measurements will avoid this problem.

Initializing a new track on every measurement is computationally expensive and requires measures to mitigate computational complexity. For this purpose, we classify the tracks as newborn, adolescent, and ordinary. Newborn tracks are tracks that have been initialized at the current time step, adolescent tracks are tracks that were initialized at the previous time step, and ordinary tracks are all other tracks. The adolescent tracks are not allowed to compete for measurements in the same way as the ordinary tracks. The restriction comes into play when an adolescent track i and an ordinary track t have gated measurement j at the current time step, and they have both gated the same measurement at the previous time step. Then, the adolescent track j is only allowed to compete for the measurement if it has a larger weight relative to the measurement than the other track

$$\max_{t,j} w_k^{tj} < T_B w_k^{ij}, \tag{99}$$

where T_B is a threshold parameter. Otherwise, the adolescent track is not allowed to compete for measurement j, which is enforced by setting $w_k^{ij} = 0$.

Termination is done as described in [37]. First, any tracks with an existence probability under a predetermined threshold T_d are removed. Furthermore, any two tracks deemed to be identical are identified by the use of the hypothesis test in [1, p. 447]. The most recently initialized of these are then terminated. Lastly, any tracks that have not been associated with a measurement for N_T radar intervals are terminated.

D. Kinematic Models

The implementation uses two different kinematic models: the constant velocity (CV) model and the coordinated turn (CT) model. Due to the varying prediction intervals, we use the discretized continuous formulation of the models. The CV model has the kinematic state $\mathbf{x} = [x, y, v_x, v_y]^{\mathrm{T}}$ where v denotes the velocity, and the state evolves according to $\mathbf{x}_k = \mathbf{F}^{(s)}(\Delta t)\mathbf{x}_{k-1} + \mathbf{v}_k$, $\mathbf{v}_k \sim \mathcal{N}(\mathbf{0}, \mathbf{Q}^{(s)})$ where

$$\mathbf{F}^{(s)} = \begin{bmatrix} \mathbf{I}_2 & \Delta t \mathbf{I}_2 \\ \mathbf{0} & \mathbf{I}_2 \end{bmatrix}, \ \mathbf{Q}^{(s)} = \begin{bmatrix} {}^{(\Delta t)^3}/_{3}\mathbf{I}_2 & {}^{(\Delta t)^2}/_{2}\mathbf{I}_2 \\ {}^{(\Delta t)^2}/_{2}\mathbf{I}_2 & \Delta t \mathbf{I}_2 \end{bmatrix} q. \tag{100}$$

Here, $\mathbf{I}$ is the identity matrix, Δt is the prediction interval, and q is the process noise intensity [2, p. 270] of the process noise. The CT model has an additional state ω, which is the turn rate. It evolves as $\mathbf{x}_k = \mathbf{F}^{(s)}(\mathbf{x}_{k-1})\mathbf{x}_{k-1} + \mathbf{v}_k$, $\mathbf{v}_k \sim \mathcal{N}(\mathbf{0}, \mathbf{Q}^{(s)})$ where

$$\mathbf{F}^{(s)}(\mathrm{x}) = \begin{bmatrix} 1 & 0 & \frac{\sin \Delta t\omega}{\omega} & \frac{-1+\cos \Delta t\omega}{\omega} & 0 \\ 0 & 1 & \frac{1-\cos \Delta t\omega}{\omega} & \frac{\sin \Delta t\omega}{\omega} & 0 \\ 0 & 0 & \cos \Delta t\omega & -\sin \Delta t\omega & 0 \\ 0 & 0 & \sin \Delta t\omega & \cos \Delta t\omega & 0 \\ 0 & 0 & 0 & 0 & 1 \end{bmatrix} \tag{101}$$

and

$$\mathbf{Q}^{(s)} = \begin{bmatrix} \mathbf{Q}^{(1)} & \mathbf{0} \\ \mathbf{0} & \Delta t q_\omega \end{bmatrix}, \tag{102}$$

where $\mathbf{Q}^{(1)}$ is a CV model covariance matrix and q_ω is the intensity of the turn rate process noise. In the implementation, the CT model is linearized as in [2, Sec. 11.7.2].

Remark 5. In most IMM applications, the transition matrix is constant. Thus, an aspect that has to be considered when the measurements do not arrive at a fixed frequency, is how to design the time-varying transition matrix $\Pi(\Delta t)$. A solution is to use the theory of Continuous Markov Chains to get an approximation for $\Pi(\Delta t)$ from the time-independent transition matrix Π. As described in [16], this can be done by use of a generator matrix G. The generator matrix is closely related to the time-independent transition matrix Π and is formulated as

(a) no transition takes place in the time interval Δt with probability $1 + g_{ii}\Delta t + o(\Delta t)$,
(b) a transition takes place in the time interval Δt with probability $g_{ij}\Delta t + o(\Delta t)$,

where g_{ij} are the individual elements of G and $o(\Delta t)$ indicates some small additional term, which is ignored.

This approximation is reasonable for relatively small Δt. Thus, the generator matrix G for M number of states can be written as

$$G = \begin{bmatrix} \pi^{11} - 1 & \dots & \pi^{1M} \\ \vdots & \ddots & \vdots \\ \pi^{M1} & \dots & \pi^{MM} - 1 \end{bmatrix}, \tag{103}$$

where π^{ij} are the individual elements of Π. Furthermore, we have from [16] that

$$\pi^{ij}(\Delta t) \approx g_{ij}\Delta t \text{ if } i \neq j \text{ and } \pi^{ii}(\Delta t) \approx 1 + g_{ii}\Delta t. \tag{104}$$

Using this, we get

$$\Pi(\Delta t) \approx \begin{bmatrix} 1 + (\pi^{11} - 1)\Delta t & \dots & \pi^{1M}\Delta t \\ \vdots & \ddots & \vdots \\ \pi^{M1}\Delta t & \dots & 1 + (\pi^{MM} - 1)\Delta t \end{bmatrix}. \tag{105}$$

E. Measurement Models

Radar Measurements

The radar measurements only contain positional data, and the measurements can be written as

$$\mathbf{z}_k = \mathbf{H}\mathbf{x}_k + \mathbf{w}_k, \quad \mathbf{w}_k \sim \mathcal{N}(\mathbf{0}, \mathbf{R}_R). \tag{106}$$

The noise matrix has both a Cartesian and polar element, to account both for errors in range and bearing, and clustering errors. The measurement noise matrix for the radar measurement becomes

$$\mathbf{R}_R = \mathbf{R}_c + \mathbf{R}_p. \tag{107}$$

Here, $\mathbf{R}_c$ is the Cartesian noise component, while $\mathbf{R}_p$ is the polar noise component converted to Cartesian coordinates. The conversion is done by using the unbiased conversion equations from [22].

Target-Provided Measurements

The target-provided measurements can contain both positional and velocity data. The kinematic part of the measurements can be written as

$$\mathbf{p}_k = \mathbf{H}^{\text{pos}}\mathbf{x}_k + \mathbf{H}^{\text{vel}}\mathbf{x}_k + \mathbf{w}_k, \quad \mathbf{w}_k \sim \mathcal{N}(\mathbf{0}, \mathbf{R}_A), \tag{108}$$

where $\mathbf{H}^{\text{pos}}$ and $\mathbf{H}^{\text{vel}}$ are the position and velocity measurement matrices, respectively. The position is usually derived from GPS information, while the velocity is derived either from a combination of speed and heading data [6]. Due to the nature of the data, we approximate the positional errors as Cartesian noise, while we approximate the velocity errors as polar noise. The measurement noise matrix for the AIS measurement becomes

$$\mathbf{R}_A = \mathbf{H}^{\text{pos}}\mathbf{R}_{c,A} + \mathbf{H}^{\text{vel}}\mathbf{R}_{p,A}, \tag{109}$$

where $\mathbf{R}_{c,A}$ is the Cartesian noise component, while $\mathbf{R}_{p,A}$ is the polar noise component converted to Cartesian coordinates, again by using [22].

Table III
Tracking System Parameters

Quantity	Symbol	unit	Value
Radar sample interval	T	[s]	2.5
Model 1 process noise intensity	$q_{a,1}$	$[\text{m}^2\text{s}^{-3}]$	0.1^2
Model 2 process noise intensity	$q_{a,2}$	$[\text{m}^2\text{s}^{-3}]$	1.5^2
Turn rate process noise intensity	q_ω	$[\text{rad}^2\text{s}^{-3}]$	0.02^2
Cartesian noise std. radar	σ_{c_R}	[m]	6.6
Cartesian noise std. AIS	σ_{c_A}	[m]	3.0
Polar range std.	σ_r	[m]	8.0
Polar bearing std.	σ_θ	[°]	1.0
Detection probability	P_{D}	[%]	92
Survival probability	P_{S}	[%]	99.9
Noncorrupted ID probability	P_C	[%]	99
Initial visibility probability	η_u	[%]	90
Visibility Markov probability	ω^{11}	[−]	0.90
Visibility Markov probability	ω^{10}	[−]	0.10
Visibility Markov probability	ω^{01}	[−]	0.52
Visibility Markov probability	ω^{00}	[−]	0.48
Gate size	γ	[−]	3.5
Clutter intensity	λ	$[\text{m}^{-2}]$	5×10^{-7}
Unknown target rate	U	$[\text{m}^{-2}]$	5×10^{-8}
Initial velocity std.	σ_v	$[\text{m s}^{-1}]$	10
Initial model probability	μ_u^s	[%]	[80 10 10]
Unknown target no ID probability	ξ_u^0	[−]	0.5
Existence confirmation threshold	T_c	[%]	99.9
Existence termination threshold	T_d	[%]	1
IMM transition probability	$\pi^{\tilde{s}s}$	[%]	$\begin{bmatrix} 99 & .5 & .5 \\ .5 & 99 & .5 \\ .5 & .5 & 99 \end{bmatrix}$

VIII. RESULTS

A. Simulation Environment

We created the simulated data in line with the assumptions in Section III. The ownship is situated at the origin and is stationary. The surveillance area is circular with a radius of 500 m. We track five targets, all appearing at the edge of the area. Three of the targets appear at time $t = 0$ s, while the last two appear at time $t = 10$ s. The data consists of true target positions, radar, and AIS measurements. The movement of the targets follows a CV model with process noise intensity $q = 0.1^2\text{m}^2\text{s}^{-3}$, with occasional maneuvers according to a CT model. Furthermore, all targets are guided toward the center of the surveillance area until they are within 50 m of it. The measurements are created according to the measurement models in Section VII-E.

The tracking parameters were tuned to achieve good performance on experimental data and are similar to the ones in [7]. We list the parameters in Table III. These are also the parameters used for creating the simulated data. The AIS measurement noise was also chosen according to the experimental data and would correspond to the measurements providing high location accuracy. Furthermore, in practical applications, the precision of the AIS location data can be dynamically adjusted according to a position accuracy flag in the AIS protocol [19].

To evaluate the results, we used five different performance measures: the optimal subpattern assignment (OSPA) metric [28], the track localization error (TLE), track fragmentation rate (TFR), track false alarm rate (TFAR), and track probability of detection (TPD). The last four evaluation methods are described in [26]. The OSPA metric provides an overall performance assessment, while the other measures provide information about specific aspects of the methods.

We tested five different methods: The three methods described in Section VI, a method using only the radar measurements, and the method described by Gaglione *et al.* in [13]. The method from [13] uses a particle filter and loopy belief propagation and is thus very different from the one described in this paper. We denote the method from [13] as the belief propagation and particle filter method (BP-PF method). The implementation uses a single CV model with process noise intensity $q = 0.7^2$ m^{2}s^{-3}, and the same parameters as in Table III where applicable. As proposed in [23], of which the method in [13] is an extension, we use 3000 particles for each potential target. We set the number of potential targets to 30, as is done in [13].

The code implementing Method A from Section VI is available at [18].

B. Simulated Data

We tested the methods on 100 simulated data sets over a range of different detection probabilities. The results are seen in Figures 2 and 3. Not surprisingly, the pure radar tracking method performs worse than the AIS-aided tracking methods from Section VI when the P_D is low. The difference becomes smaller as P_D approaches 1, but is still significant. Furthermore, we see that the method from [13] generally performs worse than all the methods in Section VI, and, in some aspects, worse than the pure radar tracking method. The right subfigure in Fig. 2 shows that the largest difference in performance is in the initial stage of the scenarios. That is, the method from [13] struggles with initialization relative to the other methods. This struggle to initialize tracks also results in significantly worse TPD, whereas the other methods perform similarly to each other.

Furthermore, the TLE of the method from [13] is better than that of the pure radar method, but it is still worse than the other methods. We see that the three methods from Section VI perform similarly. As expected, the batch processing method using added noise gives slightly less precise estimates. While we see some differences between the methods for TFR and TFAR, the errors are of an overall small magnitude. However, the pure radar tracker is more prone to track fragmentation than the other methods.

The computational complexity of the methods also warrants a comparison. The pure radar tracker is the least computationally demanding, as all the other methods add functionality in addition to performing the calculations of the pure radar tracker. The precise batch processing method is the most demanding of the target-provided measurement handling methods. This is because it requires predictions and updates for each track for each measurement. The least demanding of the three is the batch processing method with added noise, as it does not need to perform more predictions than the pure radar methods. The three methods generally do not introduce a prohibiting amount of complexity and can all be implemented using a Kalman filter. Furthermore, they are all significantly less demanding than the BP-PF method, as it uses a particle filter.

C. Experimental Data

In addition to the simulated data, the sequential measurement handling method, the pure radar tracker, and the method from [13] were tested on experimental data collected as part of the Autosea project at NTNU [8]. The data set is the same set used in [7]. We consider two scenarios, which include three different ships using AIS,

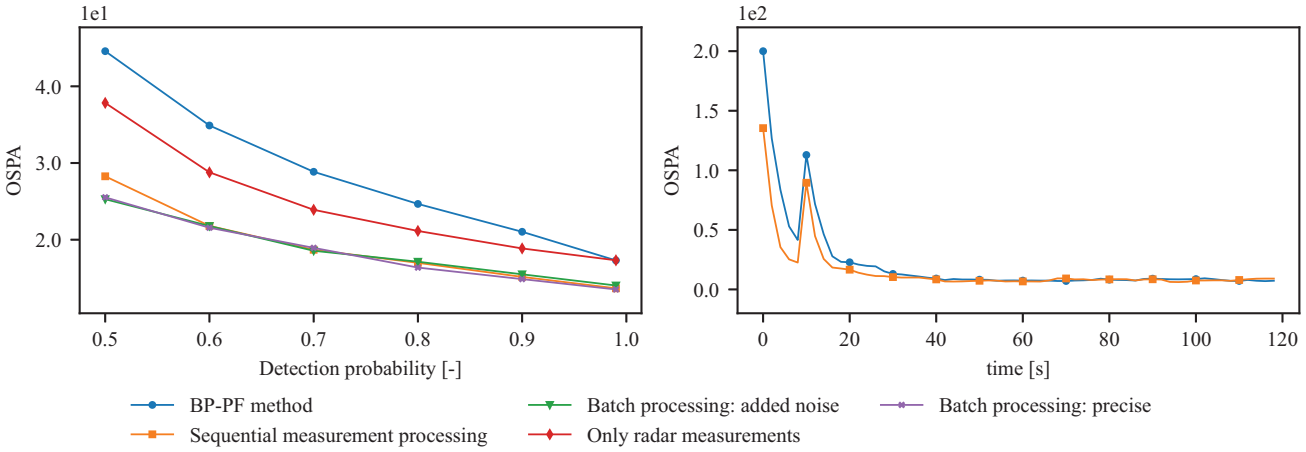

Fig. 2. Comparison of the different methods using the OSPA metric. The left figure shows the average OSPA values of each method for different detection probabilities. The right figure shows the average OSPA value for each time step, with $P_D = 0.9$. Here, we only consider the BP-PF method and the sequential measurement processing method. Both figures contain results from the same 100 scenarios. The OSPA values are calculated using $p = 2$ and $c = 200$. The purpose of the two parameters is described in [28].

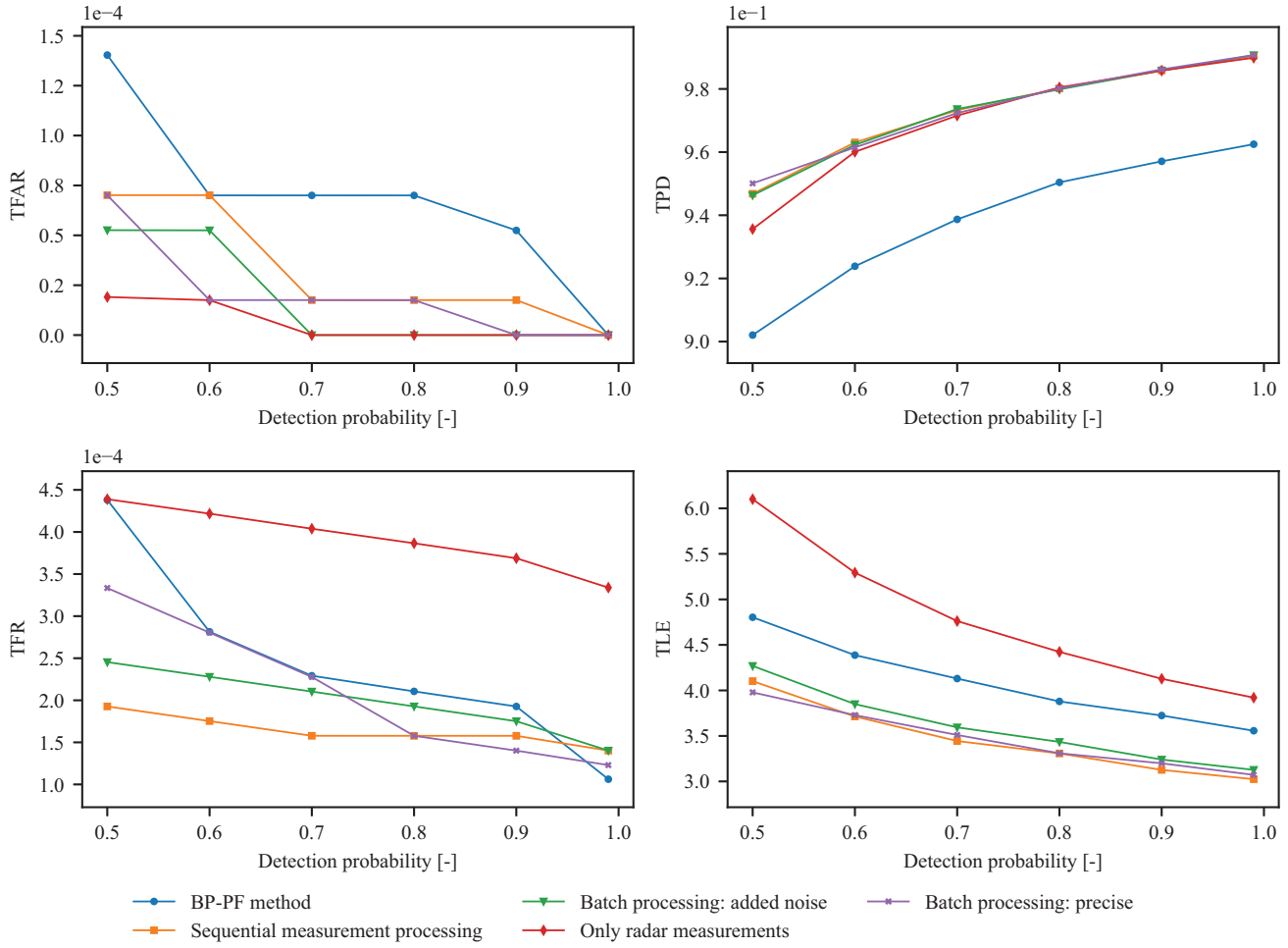

Fig. 3. TFAR, TPD, TLE, and TFR are the five different methods for different detection probabilities. The values were calculated by running the methods on the same 100 scenarios as above.

of which two provide frequent measurements. The transmission frequency for the two ships is higher than what is mandated by the IMO [19], but the data set is nevertheless helpful for demonstrating the functionality and usefulness of the tracking method. Due to the AIS data previously being used as ground truth for the AIS-equipped vessels, the AIS data has been interpolated to increase the number of measurements. This interpolation was undone prior to using the data, i.e., we removed any artificially added measurements.

Figure 4 shows the results from the first scenario. The scenario contains three fast-moving and maneuvering targets and a single slow-moving target. The slow-moving target is a large vessel with an AIS transmitter, while the three fast-moving targets are small, rigid inflatable boats (RIBs). Only one of the RIBs has an AIS transmitter, and it only transmits a single AIS measurement. The large vessel, however, provides high-quality AIS measurements. As can be seen, both the sequential measurement handling method and the pure radar method can track the scenario well, while the BP-PF method struggles. The BP-PF method likely struggles due to the kinematic modeling, i.e., because it has to use a single model to cover the kinematic behavior of both the RIBs and the large vessel. The two other methods have more flexibility in their use of IMM, and they can thus use different kinematic models for the RIBs and the large ship. When combining target-provided measurements with IMM, the tracker is also better able to select the correct kinematic model for each target. Furthermore, the sequential measurement handling method can use the AIS measurements when tracking the large vessel, improving upon the track from the pure radar method. It also correctly associates the single AIS measurement transmitted by the RIB.

The second scenario can be seen in Fig. 5. The plots show the two vessels with frequent AIS transmissions and the ownship. Figure 6 displays a close-up of the northernmost turn, with and without AIS measurements. The second scenario highlights some advantages of utilizing the AIS measurements when available. The main event occurs during the turn depicted in Fig. 6, where the radar measurements are poor due to the large vessel making a maneuver and generating numerous clutter measurements. A similar effect also occurs on the straight leading up to the turn. Both of these effects

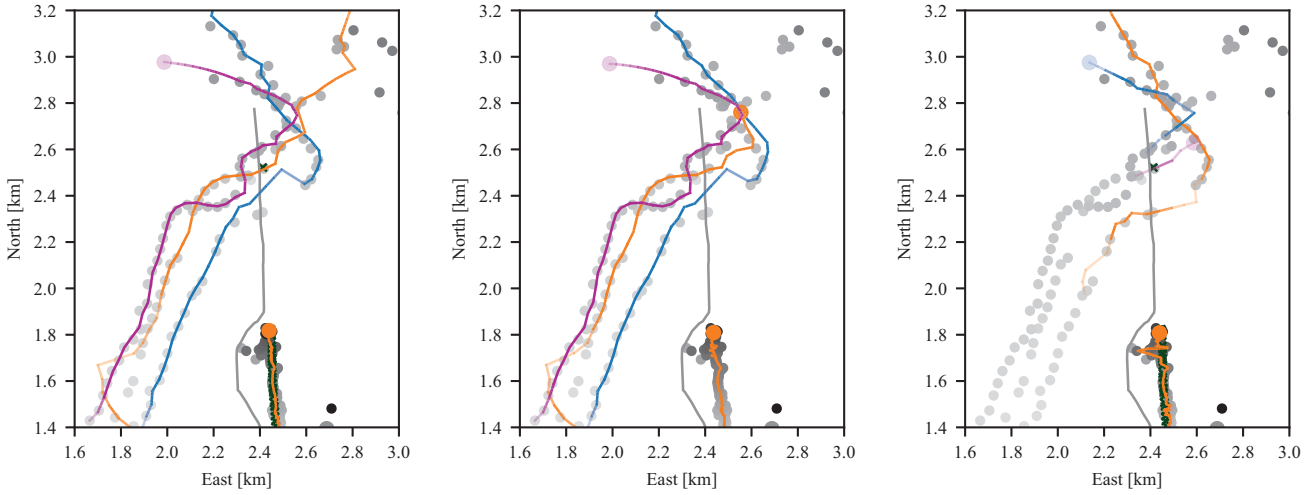

Fig. 4. A scenario showing four targets. The ownship is the gray line, moving southwards, while the targets all move northwards. The gray dots are radar measurements, and the green crosses are AIS measurements. The measurements become more transparent as time passes, i.e., the darker ones have arrived closer to the end of the scenario. The transparency of the tracks is decided by the existence probability, with the more transparent having a lower probability of existence. The target originating furthest to the right is a large vessel with an AIS transmitter, while the three other targets are small, fast-moving RIBs. Of the RIBs, only the orange has an AIS transmitter, which transmits a single measurement during the scenario. The RIBs make several maneuvers before moving beyond the radar range. (a) Results when tracking the scenario using Method A: Sequential measurement processing. (b) Results when tracking the scenario using only radar. (c) Results when tracking the scenario using the BP-PF method.

cause the purely radar-guided tracking method to veer off track, while the sequential measurement handling method can utilize the AIS measurements to avoid this. The BP-PF method loses track on the straight due to a shift in the radar measurements, combined with a temporary absence of AIS measurements, but is better able to handle the northernmost turn than the pure radar tracker. This improvement comes at the expense of a falsely initialized track on the unused radar measurements. The false track is avoided when using the sequential measurement handling method, given the correct tuning. Figure 7 shows the estimated course of the target during the turn, in addition to the standard deviation of the estimates. The poor radar measurements make the course estimates unreliable when not also utilizing the AIS measurements. When using the AIS measurements, the standard deviation of the course estimates during the turn is significant, but they are still considerably smaller than when the tracker uses only radar measurements. Furthermore, the track avoids sudden course changes. In this scenario, the inclusion of AIS measurements causes no unwanted consequences, opening the

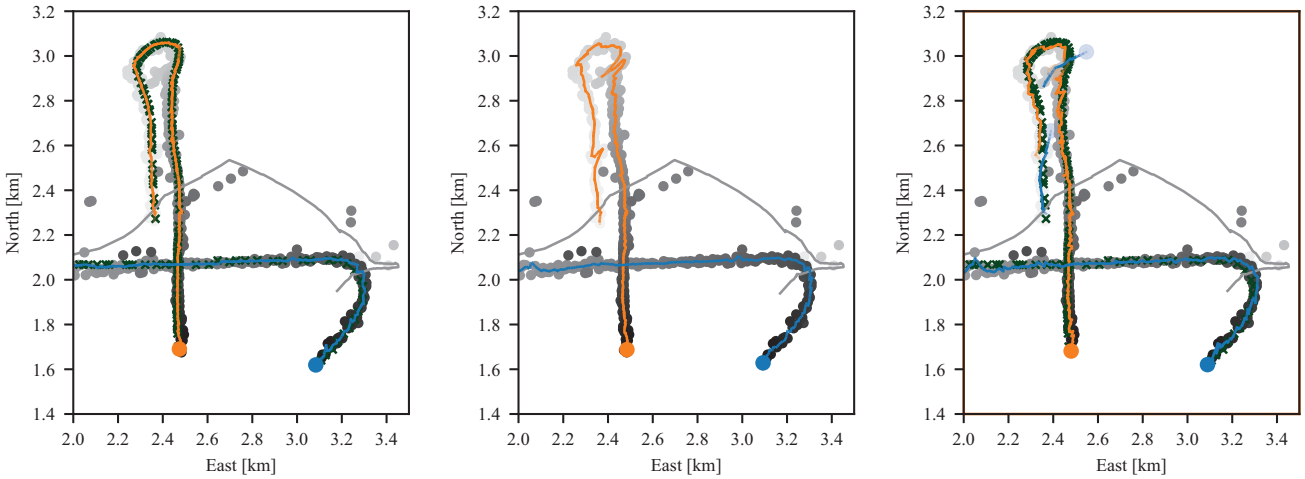

Fig. 5. A scenario showing two large vessels with AIS transmitters (with tracks shown as blue and orange lines), in addition to an ownship (gray line). We depict the measurements and tracks as in Fig. 4. Initially, the orange target moves north, while the blue target moves east. After some time, the orange target makes a u-turn, while the blue target makes a turn toward southwest. The ownship moves in a clockwise motion. The orange and blue dots represent the track positions at the end of the scenario. (a) Results when tracking the scenario using Method A: Sequential measurement processing. (b) Results when tracking the scenario using only radar. (c) Results when tracking the scenario using the BP-PF method.

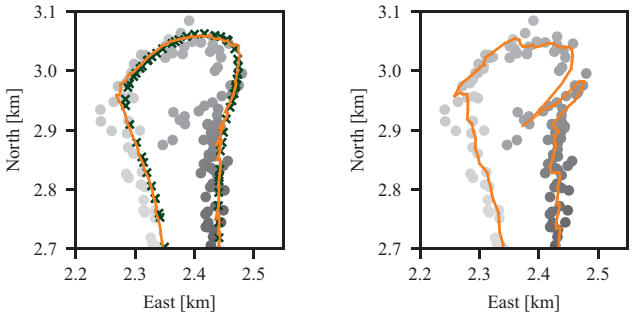

Fig. 6. A closer look at the northernmost turn for the orange track in the scenario in Figure 5. A single large vessel makes a clockwise turn, resulting in significant amounts of radar clutter. (a) A target making a clockwise turn while being tracked using AIS and radar. (b) A target making a clockwise turn while being tracked using only radar.

possibility of utilizing all the potential enhancements information given by the messages can bring.

IX. CONCLUSION

We present a framework for including target-provided measurements in a JIPDA-based tracking algorithm. We use AIS measurements as an example of such measurements. It is seen that the inclusion of such measurements can help a pure radar tracking method and improve performance greatly when the radar measurements are of low quality. In addition to the pure performance improvements, target-provided measurements can facilitate the identification of targets, which can be useful for, e.g., a collision avoidance system. Furthermore, we present and compare three different methods of handling the target-provided measurements: One method where the tracker processes the target-provided measurements when they arrive, and two methods where the tracker processes them at the time of the radar update. All three methods outperform similar state-of-the-art methods.

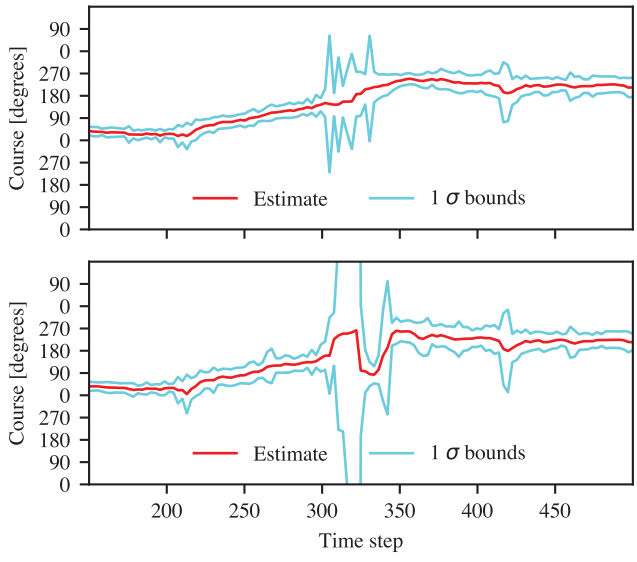

Fig. 7. Course estimate for the turn depicted in Figure 6 using both radar and AIS (top) and using only radar (bottom).

A. Future Work

The main focus of this work is how to incorporate target-provided measurements into a tracking method, and we have avoided a more thorough analysis of how to exploit the information provided by different protocols. Thus, how to use more of the data provided by such measurements should be investigated. There is also the possibility of using the expressions presented in Section V in a PMBM, which could improve performance. Another option is to use target-provided measurements to assist in clustering radar measurements. Lastly, there are safety concerns when using target-provided information. That is, the inclusion of easily manipulated input in a safety-critical system should be investigated.

ACKNOWLEDGMENT

The radar data were recorded by Erik Wilthil, Andreas Flåten, Bjørn-Olav Eriksen, and Giorgio D. K. M. Kufoalor, with assistance from Maritime Robotics and Kongsberg.

REFERENCES

[1] Y. Bar-Shalom and X. R. Li
Multitarget-Multisensor Tracking: Principles and Techniques. Storrs, CT, USA: Yaakov Bar-Shalom, 1995.

[2] Y. Bar-Shalom, X. R. Li, and T. Kirubarajan
Estimation with Application to Tracking and Navigation. Hoboken, NJ, USA: Wiley, 2001.

[3] Y. Bar-Shalom and E. Tse
"Tracking in a cluttered environment with probabilistic data association,"
Automatica, vol. 11, no. 5, pp. 451–460 1975.

[4] O. Baud, N. Honore, and O. Taupin
"Radar/ADS-B data fusion architecture for experimentation purpose,"
in *Proc. 9th Int. Conf. Inf. Fusion*, 2006, pp. 1–6.

[5] H. A. P. Blom and Y. Bar-Shalom
"The interacting multiple model algorithm for systems with Markovian switching coefficients,"
IEEE Trans. Autom. Control, vol. 33, no. 8, pp. 780–783, Aug. 1988.

[6] A. Bole, A. Wall, and A. Norris
"Chapter 5–Automatic identification system (AIS),"
in *Radar and ARPA Manual*, A. Bole, A. Wall, and A. Norris, Eds., 3rd ed. Oxford, U.K.: Butterworth-Heinemann, 2014, pp. 255–275.

[7] E. F. Brekke, A. G. Hem, and L.-C. N. Tokle
"Multitarget tracking with multiple models and visibility: Derivation and verification on maritime radar data,"
IEEE J. Ocean. Eng., vol. 46, no. 4, pp. 1272–1287, Oct. 2021.

[8] E. F. Brekke, E. F. Wilthil, B.-O. H. Eriksen, D. K. M. Kufoalor, Ø. K. Helgesen, I. B. Hagen, M. Breivik, and T. A. Johansen
"The Autosea project: Developing closed-loop target tracking and collision avoidance systems,"
J. Phys.: Conf. Ser., vol. 1357, pp. 1–12 2019.

[9] C. Carthel, S. Coraluppi, and P. Grignan
"Multisensor tracking and fusion for maritime

surveillance,"
in *Proc. 10th Int. Conf. Inf. Fusion*, 2007, pp. 1–6.

[10] K. Cutlip
Spoofing: One Identity Shared by Multiple Vessels.
Global fishing watch, 2016. https://globalfishingwatch.org/data/spoofing-one-identity-shared-by-multiple-vessels/.

[11] J. Dezert and Y. Bar-Shalom
"Joint probabilistic data association for autonomous navigation,"
IEEE Trans. Aerosp. Electron. Syst., vol. 29, no. 4, pp. 1275–1286, Oct. 1993.

[12] T. E. Fortmann, Y. Bar-Shalom, and M. Scheffe
"Sonar tracking of multiple targets using joint probabilistic data association,"
IEEE J. Ocean Eng., vol. 8, no. 3, pp. 173–184, Jul. 1983.

[13] D. Gaglione, P. Braca, G. Soldi, F. Meyer, F. Hlawatsch, and M. Z. Win
"Fusion of sensor measurements and target-provided information in multitarget tracking,"
IEEE Trans. Signal Process., vol. 70, pp. 322–336, Dec. 2022.

[14] I. R. Goodman, H. T. Nguyen, and R. Mahler
Mathematics of Data Fusion. Dordrecht, NL, USA: Springer, 1997.

[15] K. Granström, L. Svensson, Y. Xia, J. Williams, and Á. F. García-Femández
"Poisson multi-Bernoulli mixture trackers: Continuity through random finite sets of trajectories,"
in *Proc. 21st Int. Conf. Inf. Fusion*, 2018, pp. 1–5.

[16] G. Grimmett and D. Stirzaker
Probability and Random Processes. Oxford, U.K.: Oxford University Press, 2001.

[17] B. Habtemariam, R. Tharmarasa, M. McDonald, and T. Kirubarajan
"Measurement level AIS/radar fusion,"
Signal Process., vol. 106, pp. 348–57, 2015.

[18] A. G. Hem and E. F. Brekke
"Variations of joint integrated data association with radar and target-provided measurements," [source code]. Available: https://doi.org/10.24433/CO.4125751.v1.

[19] Radiocommunication Sector of ITU, "Technical characteristics for an automatic identification system using time division multiple access in the VHF maritime mobile frequency band," ITU-R M.1371-5, Recommendation ITU-R M.1371-5, Feb. 2014.

[20] X. R. Li and Y. Bar-Shalom
"Design of an interacting multiple model algorithm for air traffic control tracking,"
IEEE Trans. Control Syst. Technol., vol. 1, no. 3, pp. 186–194, Sep. 1993.

[21] E. Liland
"AIS aided multi hypothesis tracker—multi-frame multi-target tracking using radar and the automatic identification system," Master's thesis, NTNU, Trondheim, Norway, 2018.

[22] M. Longbin, S. Xiaoquan, Z. Yiyu, S. Z. Kang, and Y. Bar-Shalom
"Unbiased converted measurements for tracking,"
IEEE Trans. Aerosp. Electron. Syst., vol. 34, no. 3, pp. 1023–1027, Jul. 1998.

[23] F. Meyer, P. Braca, P. Willett, and F. Hlawatsch
"A scalable algorithm for tracking an unknown number of targets using multiple sensors,"
IEEE Trans. Signal Process., vol. 65, no. 13, pp. 3478–3493, Jul. 2017.

[24] D. Musicki and R. Evans
"Joint integrated probabilistic data association: Jipda,"
IEEE Trans. Aerosp. Electron. Syst., vol. 40, no. 3, pp. 1093–1099, Jul. 2004.

[25] D. Musicki and S. Suvorova
"Tracking in clutter using IMM-IPDA-based algorithms,"
IEEE Trans. Aerosp. Electron. Syst., vol. 44, no. 1, pp. 111–126, Jan. 2008.

[26] P. C. Niedfeldt, K. Ingersoll, and R. W. Beard
"Comparison and analysis of recursive-RANSAC for multiple target tracking,"
IEEE Trans. Aerosp. Electron. Syst., vol. 53, no. 1, pp. 461–476, Feb. 2017.

[27] J. Å. Sagild, A. G. Hem, and E. F. Brekke
Counting technique versus single-time test for track-to-track association,
in *Proc. 24th Int. Conf. Inf. Fusion*, 2021, pp. 1–7.

[28] D. Schuhmacher, B. T. Vo, and B. N. Vo
"A consistent metric for performance evaluation of multi-object filters,"
IEEE Trans. Signal Process., vol. 56, no. 8, pp. 3447–3457, Aug. 2008.

[29] M. Schuster, M. Blaich, and J. Reuter
"Collision avoidance for vessels using a low-cost radar sensor,"
IFAC Proc. Volumes, vol. 47, no. 3, pp. 9673–9678, 2014.

[30] R. L. Streit
Poisson Point Processes: Imaging, Tracking, and Sensing. New York, NY, USA: Springer, 2010.

[31] T. Tengesdal, L. M. Millefiori, P. Braca, and E. F. Brekke
"Joint stochastic prediction of vessel kinematics and destination based on a maritime traffic graph,"
in *Proc. Int. Conf. Elect., Comput., Commun. Mechatronics Eng.*, 2022, pp. 1–8.

[32] B.-T. Vo and B.-N. Vo
"Labeled random finite sets and multi-object conjugate priors,"
IEEE Trans. Signal Process., vol. 61, no. 13, pp. 3460–3475, Jul. 2013.

[33] X. Wang, S. Challa, and R. Evans
"Gating techniques for maneuvering target tracking in clutter,"
IEEE Trans. Aerosp. Electron. Syst., vol. 38, no. pp. 1087–1097, Jul. 2002.

[34] J. L. Williams
"Marginal multi-Bernoulli filters: RFS derivation of MHT, JIPDA, and association-based MeMBer,"
IEEE Trans. Aerosp. Electron. Syst., vol. 51, no. 3, pp. 1664–1687, Jul. 2015.

[35] E. F. Wilthil, Y. Bar-Shalom, P. Willett, and E. F. Brekke
"Estimation of target detectability for maritime target tracking in the PDA framework,"
in *Proc. 22nd Int. Conf. Inf. Fusion*2019, pp. 1–8.

[36] E. F. Wilthil, E. F. Brekke, and O. B. Asplin
"Track initiation for maritime radar tracking with and without prior information,"
in *Proc. 21st Int. Conf. Inf. Fusion*, 2018, pp. 1–8.

[37] E. F. Wilthil, A. L. Flåten, and E. F. Brekke
"A target tracking system for ASV collision avoidance based on the PDAF,"
Sensing and Control for Autonomous Vehicles. Berlin, Germany: Springer, 2017, pp. 269–288.

Audun G. Hem received his M.Sc. degree in engineering cybernetics from the Norwegian University of Science and Technology (NTNU), Trondheim, Norway, in 2021, and he is currently a Ph.D. student at the Department of Engineering Cybernetics, NTNU. He specializes in target tracking for autonomous surface vehicles and is currently working on the Autosit project.

Edmund F. Brekke received the M.Sc. degree in industrial mathematics and the Ph.D. degree in engineering cybernetics from the Norwegian University of Science and Technology (NTNU), Trondheim, Norway, in 2005 and 2010, respectively. From 2010 to 2014, he worked with the Acoustic Research Laboratory (ARL), NUS, Singapore, as a postdoctoral Research Fellow. In 2014, he rejoined NTNU and the Department of Engineering Cybernetics as an Associate Professor in sensor fusion. This position was funded as a gift professorship by DNV in 2014–2019. He was the Project Manager for the Autosea project, developing methods for sensor fusion and collision avoidance for autonomous surface vehicles. He is currently a Key Scientist for the Autoferry project, which is focused on autonomous pedestrian ferries, Work Package Manager in the Centre for Research-Based Innovation SFI Autoship, and the Project Manager of the Autosit and Autosight projects, which are focused on automated situational awareness for autonomous surface vehicles. He is an Associate Editor of the IEEE Journal of Oceanic Engineering. His research interests are in the area of sensor fusion and situational awareness, with a particular focus on multitarget tracking.